AD-A011 830

USE OF THE ATMOSPHERIC ELECTRIC FIELD FOR TERRAIN AVOIDANCE

C. S. Leffel, Jr., et al

Johns Hopkins University

Prepared for:

Naval Plant Representative Office

April 1975

APL/JHU
TG 1271
APRIL 1975
Copy No. 25

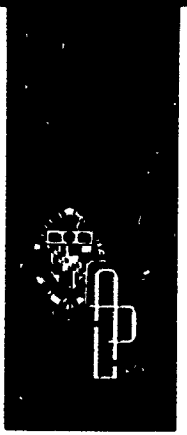

Technical Memorandum

USE OF THE ATMOSPHERIC ELECTRIC FIELD FOR TERRAIN AVOIDANCE

C. S. LEFFEL, Jr.
M. L. HILL

THE JOHNS HOPKINS UNIVERSITY • APPLIED PHYSICS LABORATORY

Unclassified

SECURITY CLASSIFICATION OF THIS PAGE

PLEASE FOLD BACK IF NOT NEEDED FOR BIBLIOGRAPHIC PURPOSES

REPORT DOCUMENTATION PAGE

1 REPORT NUMBER APL/JHU TG 1271	2 GOVT ACCESSION NO	3. RECIPIENT'S CATALOG NUMBER
4 TITLE (and Subtitle) USE OF THE ATMOSPHERIC ELECTRIC FIELD FOR TERRAIN AVOIDANCE		5 TYPE OF REPORT & PERIOD COVERED Technical Report 6 PERFORMING ORG. REPORT NUMBER
7 AUTHOR(s) C. S. Leffel, Jr. and M. L. Hill		8. CONTRACT OR GRANT NUMBER(s) N00017-72-C-4401
9 PERFORMING ORGANIZATION NAME & ADDRESS The Johns Hopkins University Applied Physics Laboratory 8621 Georgia Ave. Silver Spring, Md. 20910		10 PROGRAM ELEMENT, PROJECT, TASK AREA & WORK UNIT NUMBERS QOYO
11 CONTROLLING OFFICE NAME & ADDRESS Naval Plant Representative Office 8621 Georgia Ave. Silver Spring, Md. 20910		12 REPORT DATE April 1975 13 NUMBER OF PAGES 124
14. MONITORING AGENCY NAME & ADDRESS Naval Plant Representative Office 8621 Georgia Ave. Silver Spring, Md. 20910		15 SECURITY CLASS (of this report) Unclassified 15a DECLASSIFICATION/DOWNGRADING SCHEDULE NA
16 DISTRIBUTION STATEMENT (of this Report) Approved for public release, distribution unlimited.		
17 DISTRIBUTION STATEMENT (of the abstract entered in Block 20 if different from Report)		
18. SUPPLEMENTARY NOTES		

19 KEY WORDS (Continue on reverse side if necessary and identify by block number)

Atmospheric conductivity
Atmospheric electric field
Electrostatic stabilization
Equipotential surfaces
Electric field fluctuations
Orographic protrusion
Terrain avoidance

20 ABSTRACT (Continue on reverse side if necessary and identify by block number)

Both natural and man-made orographic protrusions perturb the normally vertical atmospheric electric field. The magnitude and direction of the electric field perturbations have been computed for such protrusions as walls and small mountains. A limited number of measurements made near ground level and from an instrumented aircraft show that the atmospheric field in the neighborhood of orographic protrusions behave as expected. From theoretical calculations of the atmospheric field and ground-based and laboratory measurements, we infer that an aircraft or missile in flight would be able to detect perturbations useful in terrain avoidance at ranges of five times the height of a typical mountain ridge if the vehicle is on a horizontal flight path lying well below the ridge altitude. The range of atmospheric and terrain conditions for which this inference is valid cannot be accurately specified on the basis of data now available.

DD FORM 1 JAN 73 1473

PRICES SUBJECT TO CHANGE

Unclassified

SECURITY CLASSIFICATION OF THIS PAGE

APL/JHU
TG 1271
APRIL 1975

Technical Memorandum

USE OF THE ATMOSPHERIC ELECTRIC FIELD FOR TERRAIN AVOIDANCE

C. S. LEFFEL, Jr.
M. L. HILL

THE JOHNS HOPKINS UNIVERSITY • APPLIED PHYSICS LABORATORY
8621 Georgia Avenue • Silver Spring, Maryland • 20910
Operating under Contract N00017 72-C-4401 with the Department of the Navy

CONTENTS

Preceding page blank

ILLUSTRATIONS

1. INTRODUCTION

The concept of using the electric field of the atmosphere for terrain avoidance had its origin in the successful use of the atmospheric electric field to stabilize the flight of model airplanes by M. L. Hill (Ref. 1). Using relatively simple electronics and servo-mechanisms, Hill showed that it was possible to fly a model aircraft or remotely piloted vehicle (RPV) along the equipotential surfaces that exist in the atmosphere parallel to the earth's surface. This "electrostatic stabilization" of flight over relatively level terrain has been demonstrated to be possible whenever the so-called "fair weather" electric atmospheric field exists – which is about 90% of the time. Since the conductivity of the ground (or any orographic protrusion) is so much greater than that of the atmosphere, the boundary condition for Laplace's, or more properly Poisson's equation describing the atmospheric potential, is that the potential at the earth's surface and the surface of any protrusion is a constant conventionally taken as zero. Thus at the earth's surface, including all protrusions, whether man-made or natural, there exists an equipotential surface, and the atmospheric field in the neighborhood of these protrusions will be distorted. The postulation of the use of the atmospheric field for terrain avoidance depends upon the detection and use of these spatial disturbances.

The first problem in this investigation was to determine the magnitude and direction of the changes in the atmospheric electric field in the space surrounding the orographic protrusion. Later in this report, it will be shown that it is possible to obtain computer solutions and in some cases analytical solutions of the atmospheric potential field in the neighborhood of realistic orographic protrusions.

Ref. 1. M. L. Hill, "Introducing the Electrostatic Autopilot," Astronautics and Aeronautics, 22-31 November 1972.

provided certain assumptions are made. These computations make it possible to specify the changes relative to the unperturbed atmospheric field in the vertical and horizontal potential gradients as a function of the horizontal distance from the protrusion at a specified altitude.

Given the results of these computations two questions exist that can only be answered by experiment. Are the assumptions made for the computations realistic enough to yield results applicable in the real world? And if the potential gradients are found to be as predicted by Poisson's equation is it possible to devise reliable instrumentation that will measure them accurately? For the limited range of parameters measured, this report will show that the answers are affirmative. The limitations in the experimental work reported are not inherent in the problem, but reflect a limited effort.

The emphasis of the present investigation has been on the atmospheric electric field at a relatively low altitude, i.e., below 150 meters. Measurements below 3 meters were made in the vicinity of the Applied Physics Laboratory in Howard County, Maryland. Measurements at higher altitudes were made of the South Mountain area in western Maryland from a Cessna 337 aircraft.

In general, the experimental program has been limited to the "fair weather" atmospheric electric field. In the study of atmospheric electricity the term "fair weather" usually refers to those occasions when the electric field vector is directed toward the earth and there is no precipitation or electrical storm activity in the area. There is a high degree of correlation between the fair weather electric field and "fair weather" in the meteorological sense, but the atmospheric electric field does occasionally change sign during meteorologically fair weather. As is shown later the fair weather atmospheric field is subject to significant fluctuations both in time and space. Although field reversals and abnormally high field strengths are usually associated with thunderstorm activity or the passage of storm fronts, these conditions have been avoided for reasons of experimental convenience. Even under the most favorable

conditions the atmospheric electric field is difficult to measure as the atmospheric potential is regarded as a very high impedance voltage source. Also, reliable measurements are quite difficult to make during periods of precipitation when insulation and triboelectric charging problems become severe. Measurements during periods of lightning activity require instrumentation of enormous dynamic range. This instrumentation must be protected against being destroyed by the high electrical field and current.

For the purposes of this investigation this restriction to the fair weather electric field is believed to be realistic since the application of the atmospheric electric field for stabilization or terrain avoidance will be much more difficult or even impossible under other atmospheric conditions. The percentage of time during which the fair weather field exists and the geographical extent over which the electric field is uniform enough to be useful are crucial questions when requirements for the mission of an aircraft or missile are involved. The sensitivity of the instrumentation required for the detection of the atmospheric electric field perturbations for purposes of terrain avoidance is a function of the dynamic capabilities of the aircraft or missile and the nature of the protrusion. These capabilities are not explicitly considered in this report.

2. THE ATMOSPHERIC ELECTRIC FIELD

Although the importance of electrical phenomena in the atmosphere was appreciated in the eighteenth century, and some significant investigations were made in the nineteenth century, the present understanding of the atmospheric electric field dates from about 1920 (Refs. 2 and 3). At about 50 km altitude, the atmosphere is (in effect) a perfect conductor; this conducting layer (the electrosphere) together with the earth forms a spherical condenser. The potential of the electrosphere is about 300 000 volts positive relative to the earth which is conventionally taken to be at a potential of zero. Therefore an electric field exists in the atmosphere that in any natural system of coordinates would be negative (i.e., pointed toward the earth) but which is usually denoted as "positive" in the study of atmospheric electricity. This confusion of sign can be avoided by referring to the atmospheric electric field as the "potential gradient." So designated, the atmospheric potential gradient is for the normal fair weather field positive in conformity with the usual conventions of electrical theory.

The flow of current between the electrosphere and the surface of the earth is carried by positive ions moving downward and negative ions moving upward. This current density is found to be constant or nearly constant as a function of altitude over any given area measured at a given time. The value of this current density is between 1×10^{-12} and 4×10^{-12} A/in^2.

Ref. 2. J. A. Chalmers, Atmospheric Electricity, Pergamon Press, New York, N. Y., 1967.

Ref. 3. H. Israel, Atmospheric Electricity, Vols. I and II, U.S. Department of Commerce, National Technical Information Service, Springfield, Va., 1973.

The conductivity of the atmosphere increases with altitude. This conductivity results in a decrease in the absolute value of the electric field with altitude since

$$\vec{J} = \lambda \vec{E} , \tag{1}$$

where λ is the conductivity. $\vec{J}$ is essentially a constant, hence $\vec{E}$ varies inversely with λ. The value of λ near the earth is typically 2×10^{-14} mho/m so that for $\vec{J} = 2 \times 10^{-12}$ A/m^2 the result is

$$\vec{E} = \frac{\vec{J}}{\lambda} = 100 \text{ V/m} . \tag{2}$$

To avoid the sign confusion inherent in atmospheric electricity, where altitude is taken as a positive coordinate, it is customary to write Eq. (2) as

$$\vec{F} = \frac{\vec{I}}{\lambda} , \tag{3}$$

where $\vec{F}$ is the potential gradient and $\vec{I}$ is a positive current density flowing toward the earth.

An obvious consequence of the decrease in the potential gradient with altitude is that the electric field has a divergence, (i.e., $\frac{\partial E}{\partial z} \neq 0$), and from

$$\nabla \cdot \vec{E} = \rho / \epsilon_o , \tag{4}$$

where ρ is the charge density, it is clear that the atmosphere is not electrically neutral but must under normal conditions contain a net positive charge per unit volume.

It is clear that the atmosphere is a conducting medium of very high resistivity. For a 1 m^2 column of the atmosphere extending from the earth's surface to the electrosphere, the columnar resistance is of the order of 10^{17}

ohms. Most of this resistance lies in the lower atmosphere, approximately one half of it below 3000 meters. A representative value of the resistivity of the atmosphere would be about 5×10^{13} ohms/m near the earth's surface.

There is a great variability in the atmospheric conductivity, and no good general law for its variation with altitude exists (e.g., see Chapter 7 of Ref. 2). A common method of fitting empirical data has been to use a series of exponentials, of which the first term predominates at lower altitudes. A typical equation, to the first power in altitude (z), would be

$$\lambda = 2.5 \times 10^{-14} \exp(0.00025z) , \qquad (5)$$

which provides a useful fit to the data for the first few thousand meters of altitude.

Since in Eq. (3) the current density is the relatively constant term, the fluctuations in $\vec{F}$ are the consequences of the fluctuations in λ. In the lower atmosphere electron lifetime is less than a microsecond, and the charge carriers are positive and negative ions. The conductivity is given by

$$\lambda = \lambda_+ + \lambda_- = n_+ e\mu_+ + n_- e\mu_- ,$$

where n_+ and n_- are the concentrations of positive and negative ions and μ_+ and μ_- are the mobilities. More properly, since there is sufficient reason to suppose that several species of ions exist at any one time, the conductivity should be written as

$$\lambda = \sum_i e(n_+\mu_+)_i + \sum_j e(n_-\mu_-)_j , \qquad (6)$$

where there are i species of positive ions and j species of negative ions. Thus the atmospheric conductivity involves two questions: first how is ionization produced and second what are the properties of ions.

At lower altitudes, the contribution to ionization by UV radiation is negligible. Over the ocean surfaces, the only source of ionization is cosmic rays. Over land, ionization is produced by ground radioactivity and by radioactive gases (principally radon) that escape from the ground. The ionization produced by ground and airborne radioactivity is very variable, but is typically several times that produced by cosmic rays in the lower atmosphere. According to Ref. 3 for the continental atmosphere the rate of ionization decreases up to an altitude of 1 km because of the decrease in earth-originated radioactivity, and increases above that altitude because of the increased effectiveness of cosmic radiation. Since the rate of ionization over land is 5 to 10 times that over the ocean, where only cosmic radiation is effective, it might be expected that the atmospheric conductivity would be much greater over continental areas. But this is not the case (in fact the conductivities over land and sea are approximately equal) because of the complex nature of the atmospheric ions and the interactions between them. Under the simple fair weather assumptions, where the electrosphere bears a relatively constant potential and the conduction current to the earth is also fairly constant, it is the wide fluctuations of the conductivity (caused by ionic phenomena) that causes the fluctuations in atmospheric potential (or potential gradient) that makes terrain avoidance or any other application of the earth's atmospheric field difficult.

There are several recognized classes of ions in the atmosphere. The so-called "small" ions are known to be more complex than a single N_2^+ or O_2^- molecule, and are thought to consist of from four to ten molecules bound in a cluster by the polarization forces exerted by the initially single charged simple molecule. The mobilities of these small ions are typically 1 to 2×10^{-4} $m^2/V\text{-}s$ or 1 to 2 $cm^2/V\text{-}s$ in the conventional CGS systems (where volts are measured in the practical or MKS system). There also exist "large" ions with mobilities between 3 and 80×10^{-4} $cm^2/V\text{-}s$. These large ions are presumably charged versions of the so-called "Aitken condensation nuclei." The large ions always result from charge transfer collisions from

small ions. There is also a class of intermediate ions that have been measured by some observers under some conditions. However, it is the Aitken condensation nuclei, which exist in large numbers over continental areas and which have meteorological significance, that produce the major complications in the discussion of ionic concentration.

If the effects of the divergence of $\vec{E}$ are ignored, then the time variation of the concentration of small and large ions can be written as follows:

Let: n_1 = number concentration of positive small ions,

n_2 = number concentration of negative small ions,

N_1 = number concentration of positive large ions,

N_2 = number concentration of negative large ions,

N_0 = number concentration of Aitken uncharged nuclei,

q = ionization rate per unit volume for small ions,

α = recombination coefficient for small ions,

η_{12} = recombination coefficient for n_1 and N_2,

η_{21} = recombination coefficient for n_2 and N_1,

η_{10} = recombination coefficient for n_1 and N_0,

η_{20} = recombination coefficient for n_2 and N_0, and

γ = recombination coefficient for N_1 and N_2.

Then the rate equation for positive small ions is

$$\frac{dn_1}{dt} = q - \alpha n_1 n_2 - \eta_{12} n_1 N_2 - \eta_{10} n_1 N_0 \qquad (7)$$

and a similar equation exists for n_2, the negative small ion. For the positive large ion:

$$\frac{dN_1}{dt} = \eta_{10} n_{10} N_0 - \eta_{21} n_2 N_1 - \gamma N_1 N_2 , \qquad (8)$$

with a similar equation for N_2. The difficulties of solving this set of equations are discussed in Ref. 2 and 3. As is the usual case in plasma physics, the uncertainties in the recombination coefficients are so large that any results are of questionable value. If, for an equilibrium solution, the time derivatives are set equal to zero, and if $\gamma N_1 N_2$ and $\alpha n_1 n_2$ are negligible and $N_1 = N_2 = N$, then it can be shown that

$$\frac{N_0}{N} = \left(\frac{\eta_{12}\,\eta_{21}}{\eta_{10}\,\eta_{20}}\right)^{1/2} \tag{9}$$

and

$$\frac{n_1}{n_2} = \left(\frac{\eta_{21}\,\eta_{20}}{\eta_{12}\,\eta_{10}}\right)^{1/2} . \tag{10}$$

In other words, the ratio of the concentration of Aitken neutral ions to charged large ions and the ratio of positive small ions to negative small ions depend upon the recombination coefficients between the small ions and the charged or uncharged Aitken nuclei.

In general, measurements show $n_1/n_2 > 1$ (1.1 to 1.5 are typical values over land) and n_1 varies from 200 to 600 cm^{-3}, the lower value associated with high values of N_0 and high pollution. Concentrations of large ions vary immensely, from 200 cm^{-3} over the ocean to 80 000 cm^{-3} in industrial areas. From Eq. (9), using accepted rates of recombination coefficients, the value of N_0/N ranges from 2 to 3. Under any conditions, the atmospheric conduction current is carried by the small ions; the effect of the Aitken condensation nuclei is that they affect the concentration of small ions. These Aitken nuclei are very large, with radii of the order of 2×10^{-6} cm. Whatever their nature, it is well established that they are most plentiful in industrial areas. The lifetime of the small ion, as deduced from Eq. (7), is from 20 seconds in industrial areas to 300 seconds over the ocean. This large difference in the lifetime of the small ion is not

reflected in the number concentration or conductivity because the generation rate of small ions is much greater over land.

The above model for the atmospheric electric field presents the picture of a spherical capacitor, with the outer shell (the electrosphere) at about +300 000 volts and a current flowing to the earth of the order of 1×10^{-12} A/m^2. Since the typical value of the potential gradient near the earth is 120 V/m, from

$$\sigma = -\epsilon_o F \ , \tag{11}$$

the charge density on the surface of the earth is

$$\sigma = -1.06 \times 10^{-9} \ \text{C/m}^2 \ .$$

For a current to the earth of 1×10^{-12} A/m^2, the time to neutralize the surface charge of the earth is

$$\tau = \frac{1.06 \times 10^{-9}}{1 \times 10^{-12}} = 1060 \text{ seconds or 18 minutes.}$$

Any method of calculating the time constant of atmospheric electricity will give a similar value, i. e., the electrosphere-earth condenser system will discharge in one-half hour or less. If the potential of the electrosphere relative to the earth is to be maintained, some mechanism must be found to maintain it. The theory generally accepted is that the atmospheric potential is caused by storm or thunderstorm activity. Although the charging-discharging balance has never been accurately demonstrated, it seems clear that the required flow of positive charge from the earth occurs during periods of electrical storm activity. This flow could be due to lightning flashes or point discharges from the earth into the intense field-reversed atmospheric regions that accompany severe electrical disturbances.

In summary, the first order attempt at a model for the atmospheric electric field posits a spherical capacitor in which the potential difference between the electrosphere and the earth is maintained by thunderstorm pumping and is run down by fair weather leakage currents elsewhere on the surface of the earth. The serious deficiencies in this model are well known (see Ref. 4), but the model remains very useful for the purposes of this investigation.

The primary objection to possible applications of the atmospheric electric field is the existence of fluctuations of considerable magnitude. Not only are field reversals observed during times of thunderstorm activity – and sometimes during periods of precipitation – but wide variations in the fair weather field are also observed. These variations occur on several time scales. There are yearly and daily variations of a nonrandom nature and random variations with time scales as short as seconds. These time variations show different characteristics over different parts of the earth's surface. The easiest atmospheric parameter to measure is the atmospheric potential or electric field, and most effort has been expended on this parameter.

Equation (3) can be written as

$$F = IR_L \ ,$$

where R_L is the atmospheric resistivity at the point of measurement. Since $I = V/R$, where V is the potential of the electrosphere and R is the columnar resistance of a 1 m^2 column of air between the electrosphere and the earth, then

$$F = \frac{V}{R} R_L \ . \qquad (12)$$

Ref. 4. H. Dalezalek, "Discussion of the Fundamental Problems of Atmospheric Electricity," Pure and Applied Geophysics (PAGEOPH), Vol. 100, No. 8, 1972, p. 43.

Differentiating Eq. (12) with respect to time and dividing the result by the same equation, the result is

$$\frac{1}{F}\frac{dF}{dt} = \frac{1}{V}\frac{dV}{dt} + \frac{1}{R_L}\frac{dR_L}{dt} - \frac{1}{R}\frac{dR}{dt} \quad . \tag{13}$$

Worldwide, the yearly fluctuation in the potential gradient is a single cycle, showing a maximum in January and a minimum in July. Daily, there is a single cycle variation with a maximum at 19 hours and a minimum at 4 hours, Greenwich Mean Time. Since the correlation of world thunderstorm activity and potential gradient is very good for the daily potential gradient variation, it is reasonable to assign the yearly and daily fluctuations of the potential gradient to the first term in Eq. (13), i.e., a variation in the potential of the electrosphere. However, these simple, single-cycle fluctuations, which are believed to be characteristics of the average worldwide field, are only observed over the oceans, the polar regions, and in isolated continental regions. In the industrialized regions of the world, where most field measurements have been made (e.g., England and Germany), the picture is much more complicated. In these locations, a two-cycle variation per day is often observed, which correlates with local time. Thus atmospheric pollution, the second term of Eq. (13), is involved. Term three of Eq. (13) is involved when R is increased by a cloud layer of large vertical and horizontal extension that reduces the current density, and consequently the potential gradient, if R_L remains a constant.

In general, the annual variation of V is about ±15% and daily variation about ±20%. These fluctuations, while by no means negligible, are small compared with the fluctuations caused by weather or pollution over industrialized continental land areas. A discussion of these fluctuations, which in general are aperiodic, is given in great detail in Chapter V of Ref. 3. Since the time constant of the atmospheric field is about 30 minutes, the existence of fluctuations with periods of a few minutes or less must be due to changes in the atmospheric conditions near the point of

measurement. As will be shown in Section 4, these local fluctuations can be very large and, on occasion, very fast.

To estimate the utility of using the atmospheric electric field for terrain avoidance, it is necessary to calculate the potential or field in the neighborhood of orographic protrusions. Since the atmospheric field has a divergence, from Eq. (4),

$$\nabla \cdot \vec{E} = \rho/\epsilon_o \ , \tag{4}$$

or

$$\nabla^2 \varphi = -\rho/\epsilon_o \ , \tag{14}$$

which is Poisson's equation for the potential φ. The usual assumption in atmospheric electricity is that

$$\nabla \cdot \vec{J} = 0 \ , \tag{15}$$

and from Eq. (1), $\vec{J} = \lambda\vec{E}$. Thus Eq. (15) becomes

$$\nabla \cdot (\lambda\vec{E}) = \vec{E} \cdot \nabla\lambda + \lambda \nabla \cdot \vec{E} = 0 \ ,$$

or

$$\nabla \cdot \vec{E} + \vec{E} \cdot \frac{\nabla\lambda}{\lambda} = 0 \ . \tag{16}$$

If it is assumed that the conductivity is a function of z (the altitude) alone, then

$$\vec{E} \cdot \frac{\nabla\lambda}{\lambda} = E_z \frac{\partial\lambda/\partial z}{\lambda} \text{ and } \frac{1}{\lambda}\frac{\partial\lambda}{\partial z} = \frac{\partial}{\partial z}(\ell n\, \lambda) \ ,$$

and Eq. (16) becomes

$$\nabla \cdot \vec{E} + E_z \frac{\partial}{\partial z}(\ell n\, \lambda) = 0 \ , \tag{17}$$

or, in terms of the potential φ,

$$\nabla^2\varphi + \frac{\partial}{\partial z}(\ell n\,\lambda)\,\frac{\partial\varphi}{\partial z} = 0 \quad . \tag{18}$$

If the conductivity is assumed to be a simple exponential function of the altitude z,

$$\lambda = \lambda_o e^{\beta z}, \text{ then } \frac{\partial}{\partial z}(\ell n\,\lambda) = \beta \quad ,$$

and Eq. (18) becomes

$$\nabla^2\varphi + \beta\,\frac{\partial\varphi}{\partial z} = 0 \quad . \tag{19}$$

Two-dimensional computer solutions of Eq. (19) have been made by Hoppel (Ref. 5) for a triangular mountain and a cliff. The computer calculations for several orographic protrusions have been performed by R. Weiss of API. These calculations include two-dimensional calculations for walls and a three-dimensional calculation for an upright pole. Kwang Yu of APL has achieved an analytic solution of Eq. (18) for a class of mountain contours (which happen to coincide very closely to the contours of typical mountains in the eastern U.S.). See Appendices A and B of this report. Both Ref. 5 and Appendix B consider effects caused by abrupt changes in the value of the atmospheric conductivity. All of the above calculations assume that the surface of the earth and the protrusion are perfect conductors.

The equipotential lines about a wall 15 meters high and 2 meters thick (computed by R. Weiss) are shown on Fig. 1. The ground-level field value at infinity is 100 V/m

Ref. 5. W. A. Hoppel, "Altitude Variations in the Electric Potential Resulting from Orographic Features," Pure and Applied Geophysics (PAGEOPH), Vol. 84, 1971, pp. 57-66.

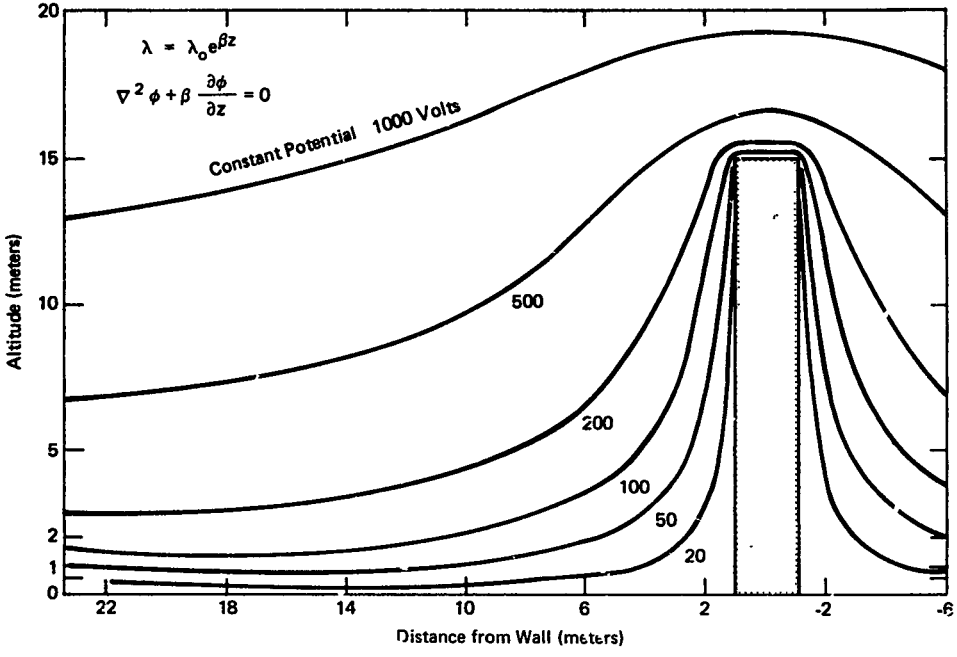

Fig. 1 Potential Contours about a Wall, 15 Meters High

and the computation is two-dimensional, i.e., the length of the wall is infinite. While the general shape of the equipotential surfaces is what one would expect, several numerical results of the plots are worth noting. If one comes toward the wall along a plane 5 meters above the ground, the vertical potential gradient decreases from 80 V/m 30 meters from the center of the wall to 19 V/m 4 meters from the wall. Along the same plane, the horizontal potential gradient is 4 V/m at a distance of 30 meters and 30 V/m at 4 meters. Moving in toward the wall on a plane 10 meters above the ground, the vertical potential gradient decreases from 79 V/m 30 meters from the wall to 60 V/m 6 meters from the center of the wall. Along the 10-meter plane, the horizontal potential gradient changes from 7.2 V/m at 30 meters to 46 V/m 6 meters from the wall. Directly above the wall, the vertical potential gradient is very large; at a height of 17 meters from the ground, the vertical potential gradient is in excess of 250 V/m. The calculated data show that at a distance of two scale heights from the wall, the horizontal gradient is rather small (less than 10 V/m) and its value is altitude dependent. Obviously, close to the ground, the horizontal gradient approaches zero. However, two useful pieces of information are available as one approaches the obstacle: the horizontal gradient increases and the vertical gradient decreases up to a point, depending upon altitude, very close to the wall.

Weiss' three-dimensional calculation for a conducting pole 5 meters high and 0.025 meter in diameter is shown in Fig. 2. Obviously, such an orographic protrusion is very difficult to detect by measurements of the perturbed atmospheric field. On the other hand, from the point of view of performing experiments, such a pole can be used to support instrumentation without greatly perturbing the local atmospheric field.

K. Yu's analytic solution for the equipotential surfaces in the neighborhood of South Mountain, Maryland is shown in Fig. 3 and discussed in Appendix A. Because the slope off this mountain is typical of the mountains in the eastern U.S., it is convenient for the experimental measurements discussed later in this report. This calculation

THE JOHNS HOPKINS UNIVERSITY
APPLIED PHYSICS LABORATORY
Silver Spring MARYLAND

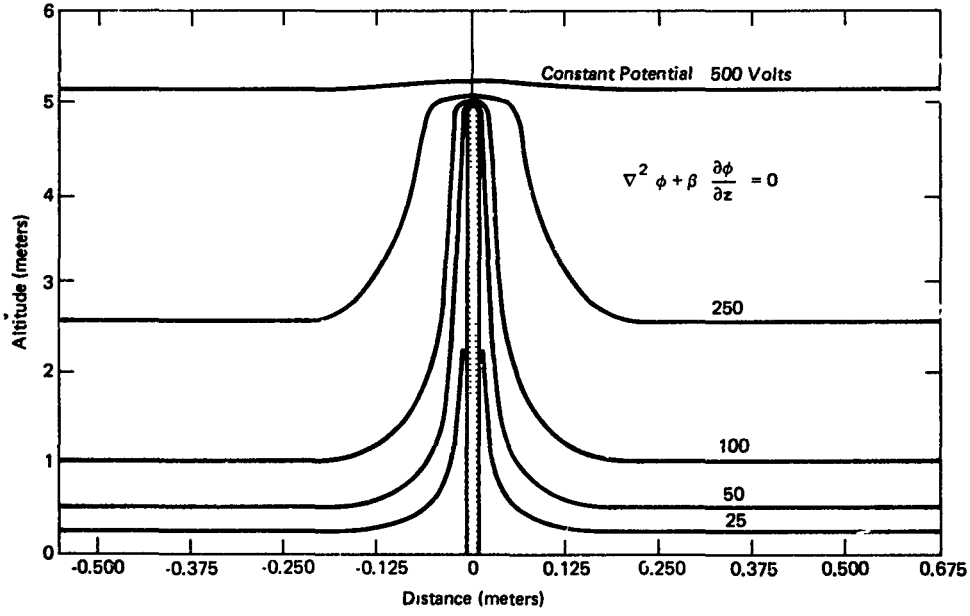

Fig. 2 Equipotential Contours about a Pole, 5 Meters High, 0.025-Meter in Diameter; Three-Dimensional Computer Calculation

was also done for a nominal electric field value of 100 V/m. At a distance of 200 meters from the ridge at an altitude of 350 meters, the horizontal field is 33 V/m. One thousand meters from the ridge at an altitude of 275 meters, the horizontal field is 5.5 V/m. Figure A4 of Appendix A shows the results of a constant contour plot for the amplitude of the electric field. If the mountain is approached on a horizontal plane lying below the mountain peak, the electric field amplitude $|\vec{E}|$ decreases until at some point (depending upon altitude) the field begins to increase. At an altitude of 300 meters the field minimum occurs about 450 meters from the ridge.

The calculations for South Mountain show that at a horizontal range of 1000 meters the horizontal gradient measured at 275 meters above sea level (110 meters above the ground) is 5.5 V/m. This mountain is 375 meters above sea level. The height of the mountain, measured relative to ground level at the range of 1000 meters from the peak, is 210 meters. Thus the horizontal gradient at the range of five times the height from the mountain is computed to be 5.5 V/m for an altitude of about one-half the mountain height. This result is sensitive to the contour of the protrusion; for the wall of Fig. 2, the horizontal gradient is at most 1.5 V/m at a range of five times its height from the wall. Further, because of the second term of Eq. (19), the solution of Eq. (19) for any protrusion must be scaled with caution. Since $\beta \approx 2.5 \times 10^{-4}$ m^{-1}, the change in conductivity with altitude is of little significance for low protrusions. Therefore, if for the same field strength, the 15-meter wall of Fig. 2 is replaced by a wall 5 meters high, the vertical and horizontal gradients will be essentially identical if measured at ranges and heights divided by a factor of 3. For the mountain in Fig. 3, if the height is increased, say by a factor of 2, and the geometric similarity of the slope is preserved, then under the assumptions made in Appendix A, the shape of the equipotential surfaces is preserved. However, value in volts of these equipotential surfaces will not precisely double for a point of geometric similarity if the unperturbed field strength remains the same. While the effects of scale changes on the values

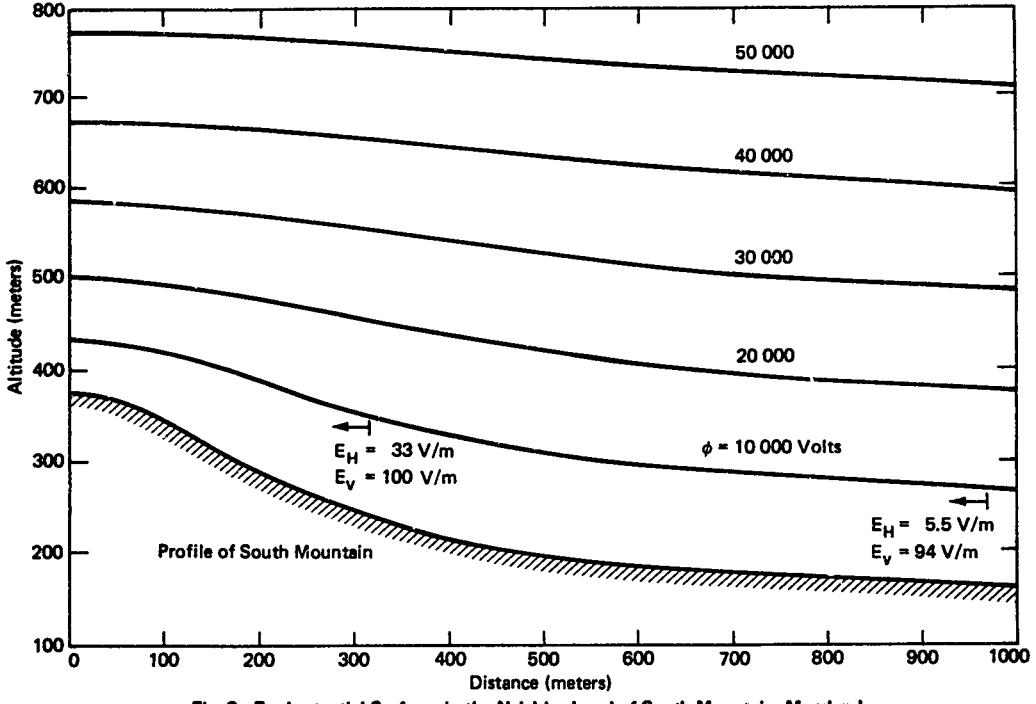

Fig. 3 Equipotential Surfaces in the Neighborhood of South Mountain, Maryland
E_o = 100 V/m

of the vertical and horizontal gradients have not been numerically computed, they will certainly be small over the altitude range for which Eq. (5) is valid. This range includes all typical mountains in the eastern U.S.

In the above calculations an exponential conductivity of the form $\lambda = \lambda_o e^{\beta z}$ is used. A question arises as to the validity of this assumption for orographic protrusions such as mountains. Hoppel (Ref. 5) has considered the effect of the change in conductivity that occurs at an inversion layer at 1400 or 3500 meters on his triangular mountain calculation for a mountain 3400 meters high by using different values of λ_o and β above and below the inversion layer. On the realistic assumption that λ_o and $1/\beta$ increase above the inversion layer, the effect is to increase the curvature of the equipotential lines above the protrusion, which would tend to aid the detection of the presence of the mountain.

In Appendix B, K. Yu considers the problem of a local semicircular region of higher conductivity located on the top of a mountain ridge. This would correspond to a situation when ground radioactivity increased the conductivity at the top of the ridge or where pollution or humidity levels decreased the conductivity in the valley. The result is a sharp jump upward in the equipotential lines at the point of discontinuity in the conductivity. While no such sharp changes in conductivity could be expected in nature, the conclusions are qualitatively correct. One would expect that the conductivity in the valleys (if it departs from the idealized exponential behavior) will be less than expected because of pollutants and thus compress the equipotential lines. In general, the slope of the equipotential lines leading into the mountain will be increased and the horizontal gradient will be increased.

In summary (from the point of terrain avoidance), it is reasonable to expect that the departure of the atmospheric conductivity from the simple exponential law can make the detection of the horizontal gradient easier.

3. METHODS OF MEASURING THE ATMOSPHERIC ELECTRIC FIELD

The most convenient atmospheric electric field parameter to measure is either the atmospheric potential or the electric field. While the atmospheric electric field is of the order of 100 V/m near the ground, the problem of measuring it is made very difficult by the fact that the atmospheric resistivity is typically 5×10^{13} ohms/m. Thus the atmospheric potential (relative to some known reference, which may be earth) requires a very high impedance voltmeter, or a true electrostatic voltmeter. The electric field may be measured directly using the relation

$$E = \sigma / \epsilon_0 \ , \qquad (20)$$

where σ is the bound charge density on a conductor in the electric field. In practice, it is necessary to mechanically modulate the field on the conductor and measure the transfer of charge (i. e., current) during the modulation process. Such a device is called a field mill.

The history and methods of measuring the atmospheric electric potential or field are reviewed in Refs. 2 and 3. The development of modern solid state electronics has ameliorated, if not eliminated, the difficulties of measurement. For these experiments, two devices were used, a high impedance voltmeter coupled to the atmosphere with a radioactive equalizer and a cylindrical field mill.

The high impedance voltmeter used in this experiment was designed at APL by R. Konigsberg (Ref. 6).

Ref. 6. R. L. Konigsberg, "Design of Portable, Solid State, High Input Impedance High Voltage Differential Electrostatic Voltmeter," submitted to Electronic Design, 13 January 1975.

This instrument uses two radioactive atmospheric couplers or sensors, usually placed a meter apart. If V_1 and V_2 are the voltages measured at the sensor positions, the signals are combined to yield:

$$V_1 - V_2 = \text{differential voltage, 0 to 500 volts}$$

$$\frac{V_1 + V_2}{2} = \text{common mode voltage, 0 to 250 volts.}$$

Figure 4 is a block diagram of this instrument. All output voltages are referenced to instrument-case ground, and the dynamic range of the instrument is limited by the high voltage supply and the high voltage emitter follower. The input impedance of the voltmeter is 10^{14} ohms or greater. The input capacity is reduced by feeding the output of the emitter follower (i.e., the sensor potential) back to the cable shielding the input and the guard plate below the radioactive equalizer. For the two instruments that have been constructed, the input capacity measures about 1 pF. The details of the radioactive sensor, guard circuit, and mounting arm are shown on Fig. 5.

The radioactive sensor used on this instrument has usually been a 500 μCi polonium 210 α emitter. Since the range of these α particles in air is about 4 cm, a relatively intense region of ionization surrounds the potential equalizer. The effective coupling impedance of such equalizers has never been precisely calculated, although values of 2×10^{10} ohms have been quoted (Ref. 2). For the present instrument, if the potential at the point read by the radioactive instrument is to be accurate, the coupling impedance to the atmosphere obviously must be much less than 10^{14} ohms. Since the time response of this instrument in the atmospheric field or a laboratory field is measured to be less than 1/2 second (and is probably faster than the recorder used in the measurement) from the 1 pF input capacity, the coupling impedance is certainly less than 5×10^{11} ohms. Therefore, the inherent error of this instrument in measuring the atmospheric potential is negligible.

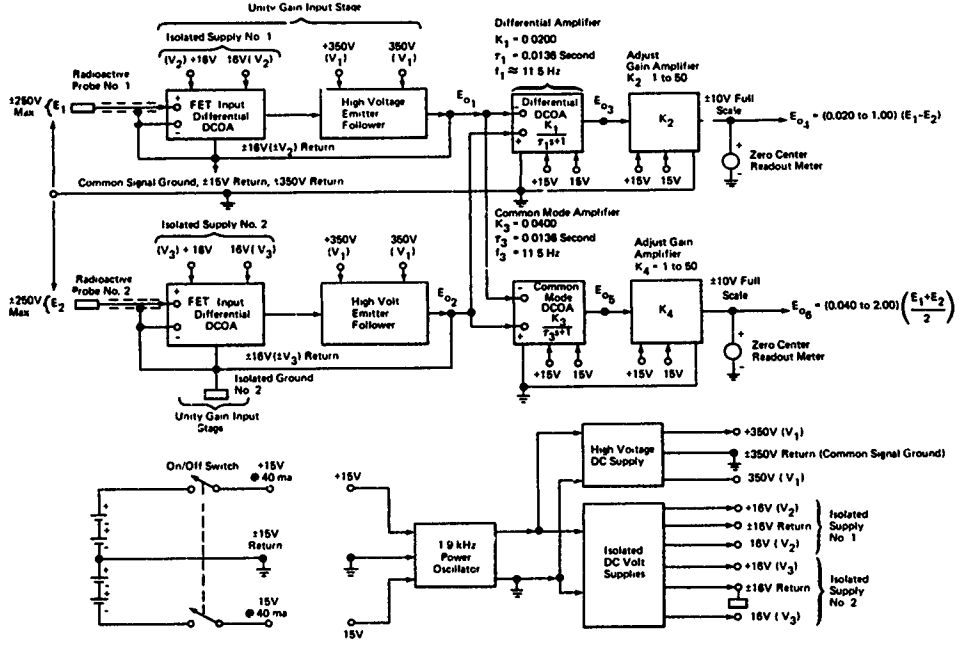

Fig. 4 Block Diagram of a Portable High-Voltage, High-Impedance Electrostatic Voltmeter

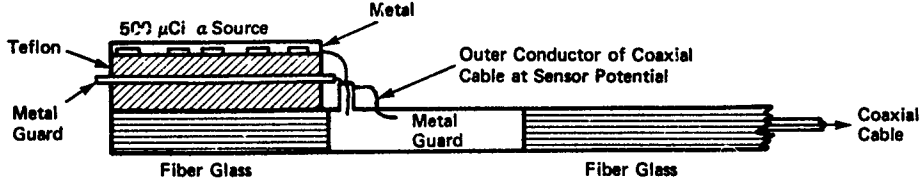

Fig. 5 Radioactive Potential Equalizer for High Impedance Voltmeter; Metal Guards Are Connected to Feedback Circuit of Voltmeter for Maintenance at Equilizer Potential

The cylindrical field mill used in this experiment was one constructed by H. W. Kasemir (Ref. 7) and loaned to APL by the Army Electronics Command (ECOM), Ft. Monmouth. While simple in principle, the field mill is complicated mechanically and expensive to construct. Figure 6 is a greatly simplified schematic of the cylindrical field mill. The mill consists of an insulated split cylinder. This cylinder is supported by a base and rotated by a small motor within the base. Using an infinite cylinder approximation, the charge on the top segment of the cylinder is given by (Ref. 6)

$$Q = -4\epsilon_o EaL \sin \varphi_1 \ ,$$

where E is the electric field, a and L the radius and length of the cylinder, and φ_1 the angle between the vector $\vec{E}$ and the insulated strip between the segments of the cylinder. If the cylinder rotates with an angular velocity ω, then the current flowing between the segments is

$$I = -4\epsilon EaL\omega \cos (\omega t + \varphi_1) \ .$$

The voltage output of an operational amplifier with a transfer impedance of R, mounted between the cylindrical segments is

$$U_o = -IR = 4\epsilon EaL\omega R \cos (\omega t + \varphi_1) \ . \qquad (21)$$

For this field mill, a = 5 cm, L = 10 cm, R = 22×10^6 ohms, and the frequency of revolution is 1800 rpm. Thus for an electric field of 100 V/m the peak value of U_o is 77 mV. The output of the operational amplifier (mounted inside the revolving cylinder) is taken from a slip ring and rectified by a phase sensitive rectifier locked to the angle φ_1. The rectified signal is amplified and recorded. A complicated set of slip rings (not shown on Fig. 6) is

Ref. 7. H. W. Kasemir, The Cylindrical Field Mill, AD-610485, ECOM, Ft. Monmouth, N. J., 1964.

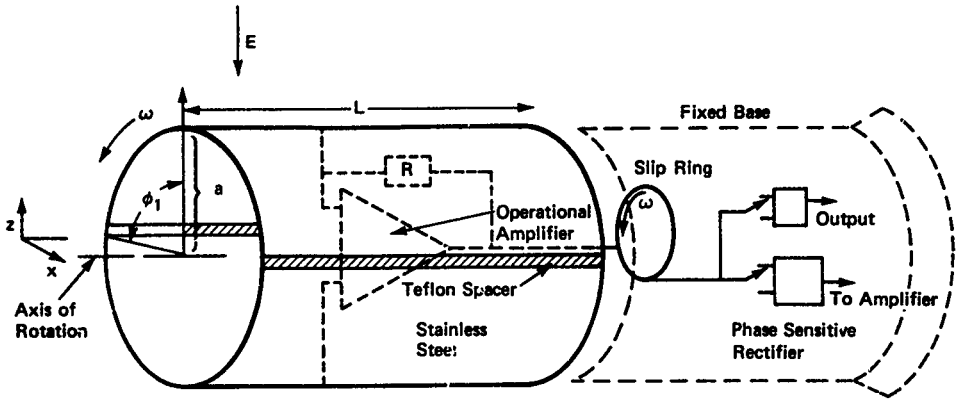

Fig. 6 Schematic Diagram of Cylindrical Field Mill

required to supply power to the current amplifier and provides the phase information for the rectifier. By using two phase-locked amplifiers, phased 90° apart, both the x and z components of the electric field can be recorded simultaneously. The calibration of the field mill and the orientation of its base to give orothogonal vertical and horizontal field measurements were performed in the laboratory by placing the mill between 1 m^2 capacitor plates 1.64 meters apart. The dynamic range of the field mill is very large; for a single value of R = 22 megohms, the field mill will record field values of from 25 to 1250 V/m full scale, and the value of R can be remotely switched to record fields of the order of 100 000 V/m. Thus, with a good recorder, field values as low as 0.25 V/m can be recorded. Unfortunately, the z and x gain channels of this field mill cannot be set at separate values with the present electronics. However, overdriving one channel does not affect the other.

Whatever method is used to measure the atmospheric field, the instrument must be supported in the atmosphere and the data recorded. This support system necessarily produces some distortion in the atmospheric field. Further, the observer must remain some distance from the measuring apparatus since he is an orographic protrusion and his clothing is usually electrostatically charged.

For measurements with the high impedance voltmeter, the support stand shown in Fig. 7 was used. The vertical support rods were always grounded; the horizontal bar supporting the voltmeter was either grounded or operated at a positive bias with respect to ground. If the positive bias is set to a value so that the common mode voltage of the meter is zero, then the support bar and meter case are at local atmospheric potential and very little perturbation of the local field occurs. Meter readings were either taken from a distance with a telescope or recorded on an accurate potentiometer-type recorder mounted on the ground 15 or 20 feet away from the instrument. When

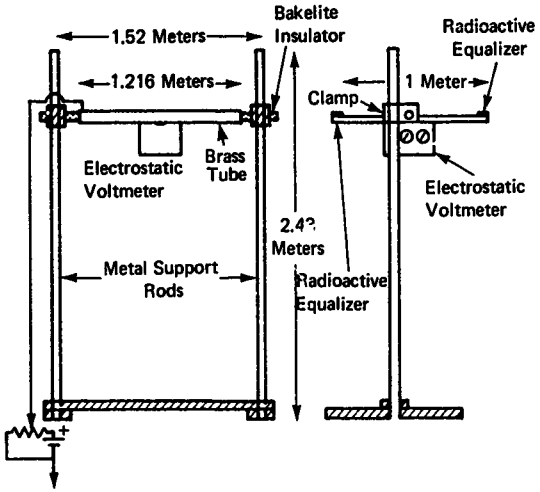

Fig. 7 Support Stand for Electrostatic Voltmeter

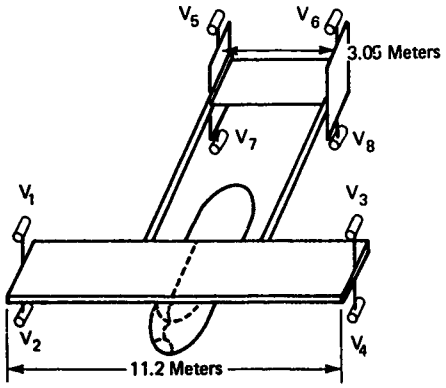

Fig. 8 Position of Atmospheric Potential Field Sensors on Cessna 337 Airplane

the case of the instrument is biased to atmospheric potential, the output signal of the meter must be isolated from ground. The recorder used for these measurements has a double-ended input that provides about 600 volts isolation from ground. The recorder accurately indicates the difference voltage applied across its terminal. A signal isolator was constructed and used occasionally for converting the DC meter output into a pulse-width modulated signal. This signal was used to drive a light-emitting diode diode. The light signal was detected and integrated, yielding a signal referenced to ground that was identical to the input signal. This device provided isolation for at least 1500 volts. In general, with a ground-based recorder, one is limited to heights of less than 10 meters.

Aircraft measurements of the atmospheric field were made with an instrumented Cessna 337 aircraft. Radioactive potential equilizers were mounted on the wing tips and tail rudders (Fig. 8). Each sensor was mounted about 0.5 meter from the metal skin of the aircraft. Sensors 1 through 6 were connected to the high impedance voltmeter circuit (Fig. 4), and the signals could be combined in the following modes: $(V_1 + V_2)/2$, $V_1 - V_2$, $(V_3 + V_4)/2$, $V_3 - V_4$, $(V_1 + V_3)/2$, $V_1 - V_3$, $(V_2 + V_4)/2$, $V_2 - V_4$, $(V_5 + V_6)/2$, and $V_5 - V_6$. Sensors 7 and 8 were connected to a low impedance autopilot circuit (described in Ref. 1) and could be combined to yield $(V_7 + V_8)/2$ and $V_7 - V_8$. During flight the processed sensor signals were recorded on magnetic tape (20 channels available), and two channels were available on a strip recorder. For the flights covered in this report, not all of the above signal combinations were available at one time because of a lack of operational amplifier summing and differencing channels. For example, for the wing sensors $(V_1 + V_2)/2$, $V_1 - V_2$, $(V_3 + V_4)/2$, and $V_3 - V_4$ could be recorded simultaneously. By throwing a switch, the signal processing could be changed to record $(V_1 + V_3)/2$, $V_1 - V_3$, $(V_2 + V_4)/2$, and $V_2 + V_4$. The aircraft was also equipped with a vertical gyro so that bank and pitch angles could be recorded. The pods, which contained instrumentation to measure conductivity, were

mounted under each wing. Various flight parameters such as air speed, altitude, and temperature could also be recorded. However, the aircraft instrumentation was primarily dedicated to the ECOM-sponsored RPV program; for the purposes of terrain avoidance, the signals of primary importance were from the wing and tail atmospheric potential sensors.

Measurement of the atmospheric potential from an aircraft faces two difficulties: (a) the potential at the sensor position must be referenced to something, usually the aircraft skin, and (b) there is a distortion in the potential field caused by the presence of the conducting skin of the aircraft.

It is well known that the aircraft skin can, under certain conditions, become charged to very high potentials (hundreds of thousands of volts) relative to the ambient atmospheric potential. The perturbation of the potential field caused by a conductor can be calculated analytically, but these calculations are limited to those few simple shapes for which Laplace's equation can be solved. As a consequence, the "form factors" for the potential field or the "augmentation factors" for the electric field must be determined experimentally.

The difficulties of measuring the atmospheric potential from an aircraft are closely related to the problem of the electrostatic autopilot. This situation is covered in Appendix C, where the potentials and fields in the neighborhood of conducting spheres and prolate spheroids are discussed. For the case of the conducting sphere, using the coordinate system of Appendix C, the potential outside the sphere is given by

$$\varphi = \varphi_o \left(1 - \frac{r_o^3}{r^3}\right) + \varphi_s \frac{r_o}{r} \quad ,$$

where φ_o is the atmospheric potential and φ_s is the potential on the surface of the sphere caused by self-charge. If a voltage sensor is placed outside the sphere, reading the atmospheric potential relative to the skin of the sphere, then that sensor will read a voltage given by

$$V_1 = \varphi_o \left(1 - \frac{r_o^3}{r^3}\right) + \varphi_s \left(\frac{r_o}{r} - 1\right) .$$

The case of the prolate spheroid leads to results of a similar form and, in general, a sensor mounted off the skin of the aircraft will measure a voltage given by

$$V_1 = \varphi_{o1} \left(1 - \alpha_1 (\vec{r}_1)\right) + \varphi_s \left(\beta_1 (\vec{r}_1) - 1\right) , \qquad (22)$$

where $\alpha_1 (\vec{r})$, which is a function of the aircraft surface shape and the location of the sensor, is the perturbation caused by the charge induced on the aircraft skin by the atmospheric field; $\beta_1 (\vec{r}_1)$ is the similar factor for the potential field caused by any self-charge on the aircraft. $\beta_1 (r_1)$ is a fixed function for any coordinate system fixed in the aircraft, but $\alpha_1 (\vec{r})$ is a function of aircraft position. Calculations for the sphere show (if the analytic expression for the potential is derived for $\varphi_o = 0$ at the center of the sphere) that convention for the assigning of values for the atmospheric potential must be preserved for all calculations.

It is clear from Eq. (22) that for a high impedance voltmeter coupled to the atmosphere with a radioactive potential equalizer (that reads the atmospheric potential at its location relative to φ_s), if φ_s is large enough the signal V_1 will saturate the amplifier. (For sensors located off the skin, $\alpha_1 (r)$ and $\beta_1 (r)$ are always less than one.) Furthermore, because the dynamic range of this high impedance instrumentation is $V \approx 250$ volts for any sensor, the atmospheric field is often greater than 100 V/m and the dimensions of the aircraft are several meters, the point in the atmosphere at which φ_s coincides with the atmospheric potential is very important. For example, if

the atmospheric potential coincides with the skin potential for a point low on the aircraft skin, the sensors mounted above the top of the wings can easily saturate their amplifiers. If V_1 saturates, no signal processing such as $V_1 - V_2$ can yield a valid result, even though $V_1 - V_2$ is well within the dynamic range of the instrument.

Early in the history of the flights with the Cessna 337, it was realized that such saturation effects did indeed occur. The analysis of experimental data was consistent with the fact that the aircraft skin potential assumed an atmospheric potential for a point low on the aircraft frame. Presumably this point coincides closely with the engine exhausts. In general, for fair weather flights, no high values of φ_s have been observed. It has been necessary, however, to provide a method of biasing the aircraft frame so that signals such as $V_1 - V_3$ could be measured over a range of bank angles. This was accomplished by mounting a conducting sheet to the aircraft skin behind the exhaust of the front engine. For example, by applying up to 1000 volts on this conductor it is possible to set the skin potential so that V_1 is nearly zero, or if the experiment requires it, making V_1 positive and V_2 negative. The only way to assure that saturation does not occur is to measure the output of each sensor individually before it is processed. For each flight the skin bias must be adjusted to a value to assure nonsaturation for all the sensors relevant to the test plan for that flight.

For most of this experimental work, both on the ground and in the air, the high impedance voltmeter coupled to the atmosphere with a radioactive potential equalizer has been used. Problems inherent in the use of radioactive equalizers have been recognized for some time (Refs. 2, 3, and 8). Unfortunately, no general theory of the radioactive potential equalizer exists. Recently, M. L. Hill and

---

Ref. 8 R. Wagner, "Zur Messung des luftelekrishen Potentialgefälles mittels Kollektoren," Archiv für Meteorologic, Geophysik und Bioklimatologic, Series A, Vol. 3, No. 4, 1955, pp. 427-463.

W. A. Hoppel (Ref. 9) of APL analyzed the performance of the radioactive equalizer to a greater degree than had been previously done. Their emphasis was placed primarily on the autopilot circuit for RPV's. These are relatively low impedance circuits, and since the coupling of the sensor to the atmosphere is a higher impedance than that presented by the amplifier, the autopilot circuit and the radioactive equalizer are best treated in a current source mode. The difference signal between the right and left wing sensors, for example, is approximately given by

$$i_L - i_R = 2GAE_z \sin\theta \ ,$$

where θ is the bank angle of the aircraft, E_z is the vertical electrical field, A is the electric field augmentation factor, and G is the gain of the electric field sensors and the associated electronics. The conclusions, which are well supported by experiment, are that the current flow through the sensor is determined by the atmospheric electric field, the radioactivity of the α source, the dimensions of the source, and the air velocity flowing over the source. The theory does not work for zero air velocity, and for the realistic cases they consider, the current tends to become independent of air velocity for air speeds above 20 mi/h. Thus they substantiate what numerous RPV flights have shown, that the equalizer in its current operating mode is a reliable indicator for the atmospheric field as long as the radioactivity is not reduced by water or oil on the surface of the α emitter.

For the case of the radioactive equalizer connected to the high impedance voltmeter, Hill and Hoppel (Ref. 9) show that, for a cylindrically symmetrical ionizer, the

---

Ref. 9. M. L. Hill and W. A. Hoppel, "Effects of Velocity and Other Physical Variables on the Currents and Potentials Generated by Radioactive Collectors in Electric Field Measurements," presented at the Fifth International Conference on Atmospheric Electricity, Garmisch-Partenkirchen, West Germany, 2-7 September 1974.

ionizer assumes the correct atmospheric potential provided the net current drawn from the sensor is essentially zero. This result is independent of the air velocity over the sensor. If the sensor is not symmetrical about its axis perpendicular to the atmospheric field, a positional error is produced. This error is of the order of the displacement produced by the highly conducting sheath about the radioactive probe. In practice it is relatively small since the high conductivity region extends for only a few centimeters They further show that if the equalizer has an initial charge or if one is imparted to it, the time constant for the equalizer to reach equilibrium is

$$\tau = \epsilon_o/\lambda \qquad (23)$$

where λ is the conductivity in the highly conducting region. Since in this region λ is orders of magnitude greater than its atmospheric value of 10^{-14} mho/m, τ can be expected to be less than 1 second. From Ref. 9, a conservative estimate of τ is 0.2 second for a 500 μCi α source. τ is a function of the radioactivity of the source; however, the voltmeter reading is not as long as the sensor coupling impedance to the atmosphere is much less than the input impedance of the meter.

4. RESULTS OF THE EXPERIMENTAL PROGRAM

NOISE ON THE HIGH IMPEDANCE VOLTMETER

When the high impedance voltmeter was mounted on the support structure and the common mode and differential signals recorded, one of the surprising results was the high noise level on the differential signal (see Fig. 7). The voltmeter was usually mounted with the arms supporting the radioactive sensors in a horizontal position, consequently the common mode signal $((V_1 + V_2)/2)$ was a measure of the vertical field and the differential signal measured the horizontal gradient. Figure 9 shows an example of the fluctuations observed. These data were recorded on the flat roof of an APL building in Howard County, Maryland; the departure of the average differential readings from zero is explained by the fact that the voltmeter was mounted close to one edge of the flat roof.

The Fig. 9 data were recorded on consecutive days and, even though the field strengths are comparable, the fluctuations for the second day are much greater; and exceed ±10 volts about the average for the differential channel. The weather conditions were different and may be summarized as follows

	6 June 1974	7 June 1974
Temperature (°C)	26	15.5
Relative humidity (%)	30	69
Wind velocity (mi/h)	0-2	4-5, gusty
Barametric pressure (mb)	1010	1011
Cloud cover	Clear, sunny day	Overcast, threatening

It is difficult, however, to find any reliable correlation between meteorological data and the measured fluctuations. Figure 10 shows data that were recorded on a clear day. The wind velocity was from 10 to 20 mi/h. These data are very noisy. The data shown in Fig. 9 were recorded with the sensors 1 meter above the roof surface; for the data shown in Fig. 10 the sensors were 1.36 meters high, and thus the average vertical electrical field is about 37%

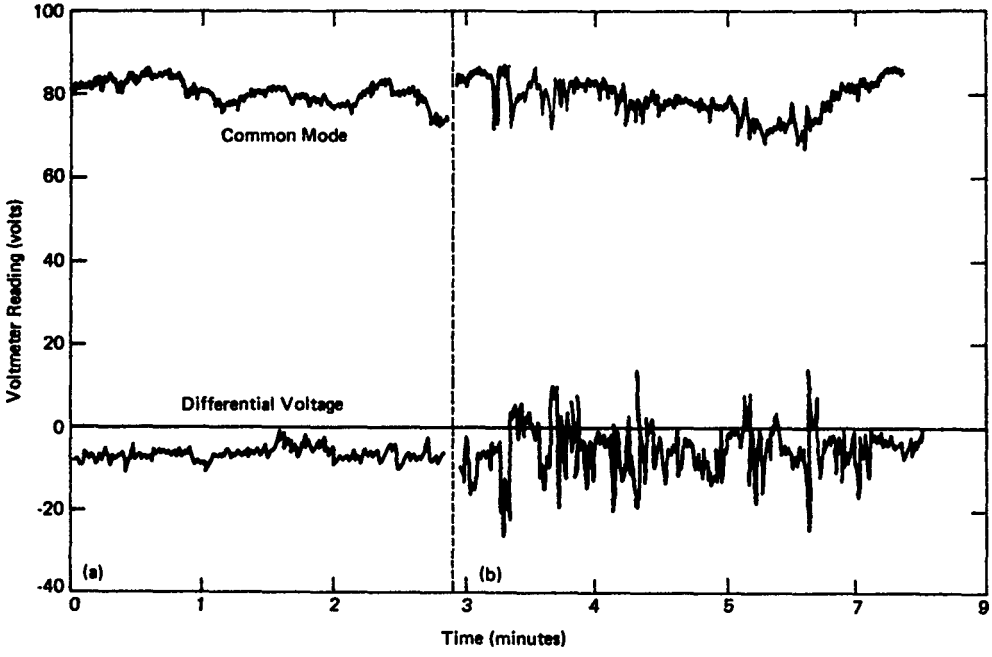

Fig. 9 Common Mode and Differential Voltage Readings versus Time, High-Impedance Voltmeter (a) 6 June 1974, (b) 7 June 1974

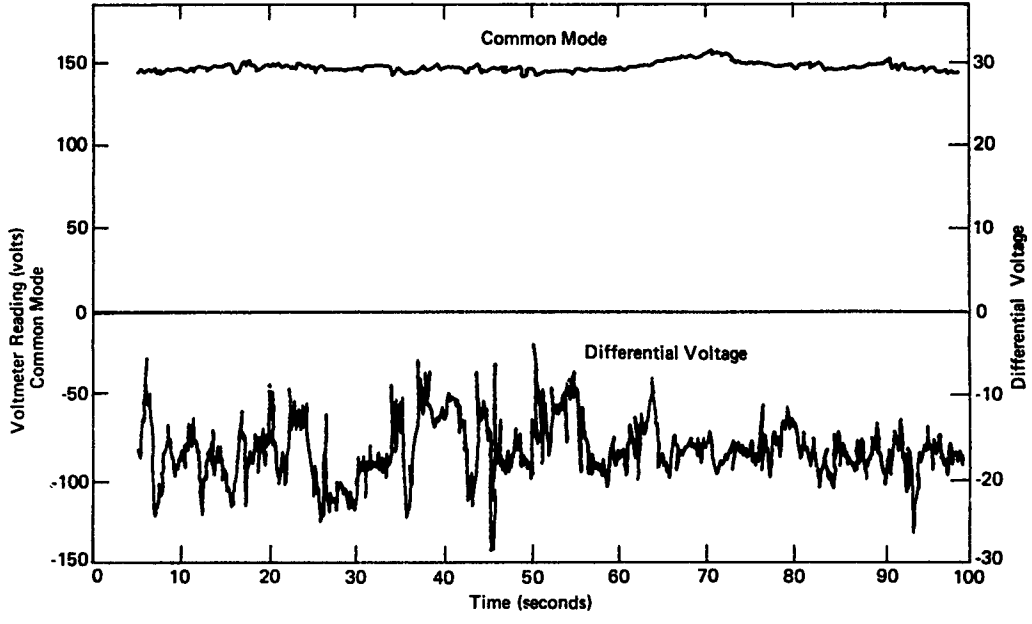

Fig. 10 Common Mode and Differential Voltages versus Time, High-Impedance Voltmeter

higher. Figure 10 is recorded on a faster time scale to show the high speed (< 1 second) of the fluctuations.

Battery voltages applied to the sensors through 10^{11} ohm resistors proved that the battery-powered high impedance voltmeter has negligible internal noise: readings taken in open fields showed that the above fluctuations are not caused by the local laboratory environment. Readings taken with the sensors at altitudes of from 1 to 4.5 meters show no significant difference. The fluctuations are definitely coupled into the voltmeter through the radioactive sensors, but the question remained as to whether the fluctuations were characteristic of the atmospheric electric field or were the result of some interaction between the radioactive potential equalizer and the atmosphere.

The data shown in Figs. 9 and 10 were taken with the high impedance voltmeter case grounded; that is, the voltmeter was connected to the recorder by shielded cable with the cable shield connected to the instrument case and grounded at the recorder. This distorts the atmospheric field about the instrument and produces an error in the atmospheric potential reading at the sensor position. Isolating the recorder input from ground and biasing the voltmeter case to near atmospheric potential increases the atmospheric potential as read at the sensor and, for all the cases in which this has been done, decreases the differential fluctuations. An example of these effects is shown in Fig. 11. The sensors were 1.27 meters above the flat roof top. For the grounded voltmeter, the common mode reads about 105 volts; when biased to near atmospheric potential (i.e., common mode near zero), the instrument bias reads about 155 volts. Thus the high impedance voltmeter, when operated with its case grounded, reads about 67% of the true atmospheric potential. While biasing the high impedance voltmeter to atmospheric potential does not eliminate the fluctuations in the horizontal gradient (the differential signal), the reduction in their amplitude has always been found to be significant.

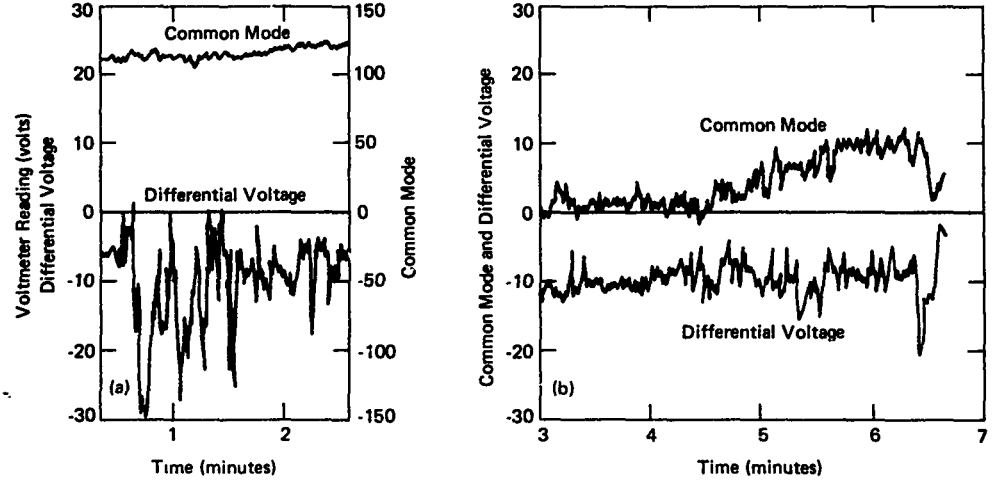

Fig. 11 Common Mode and Differential Voltages versus Time, High-Impedance Voltmeter (a) with Voltmeter Case Grounded and (b) with +150 Volt Bias on Voltmeter Case

In an attempt to determine the origin of these fluctuations, a series of laboratory measurements was made with the high impedance voltmeter. In the laboratory, the atmospheric electric field does not exist. To generate a field, the meter sensors were placed between 1 m^2 metal plates, 1.64 meters apart, and the top plate was connected to a precision high voltage supply. When voltage was applied between the plates, fluctuations appeared on the voltmeter outputs and increased in amplitude as the electric field was increased. The fluctuations were similar to those observed in the atmosphere, except that their frequency was somewhat lower. In the laboratory the potential across the capacitor plates does not fluctuate and the electric field in the absence of the sensor cannot fluctuate. It was suspected that the fluctuations recorded above are (at least in part) spurious in the sense that they do not measure the atmospheric field accurately.

This was confirmed by comparing the high impedance voltmeter with the cylindrical field mill. Figure 12 shows a comparison of field mill and the high impedance voltmeter readings when they were placed between capacitor plates in the laboratory. While the high impedance voltmeter shows its characteristic fluctuations, the field mill is essentially free of fluctuations. The difference of scale shown on Fig. 12 is not significant; the field mill and its support were calibrated between the capacitor plates and the measured electric field is correct by definition. The high impedance voltmeter reads potential, not field, and its reading depends on how high it is placed from the bottom capacitor plate. An additional uncertainty is produced because the sensors extend into the fringing region of the capacitor plates. Thus it would appear that the fluctuations are caused by some interaction of the radioactive source and the air when in an electric field. This is proven in Fig. 13, where the vertical and horizontal field strengths measured by the field mill are recorded with and without a 500 μCi α source suspended 10 cm from the side of the field mill. When the field mill was mounted outside in the atmosphere it did not show the fluctuation characteristic of the high impedance voltmeter. Figure 14 illustrates the readings of

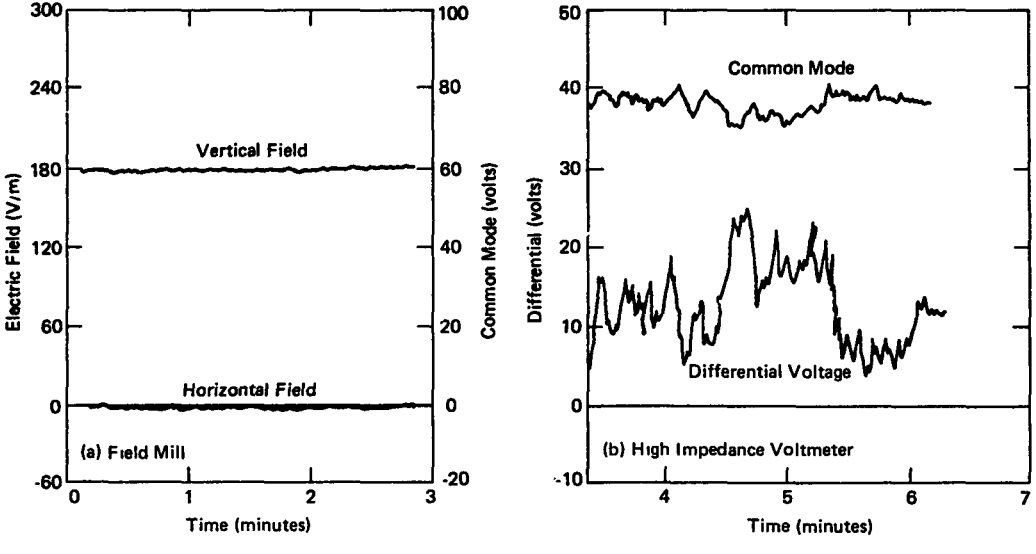

Fig. 12 Laboratory Comparison (a) Field Mill with 295 Volts on Capacitor Plates and (b) High-Impedance Voltmeter

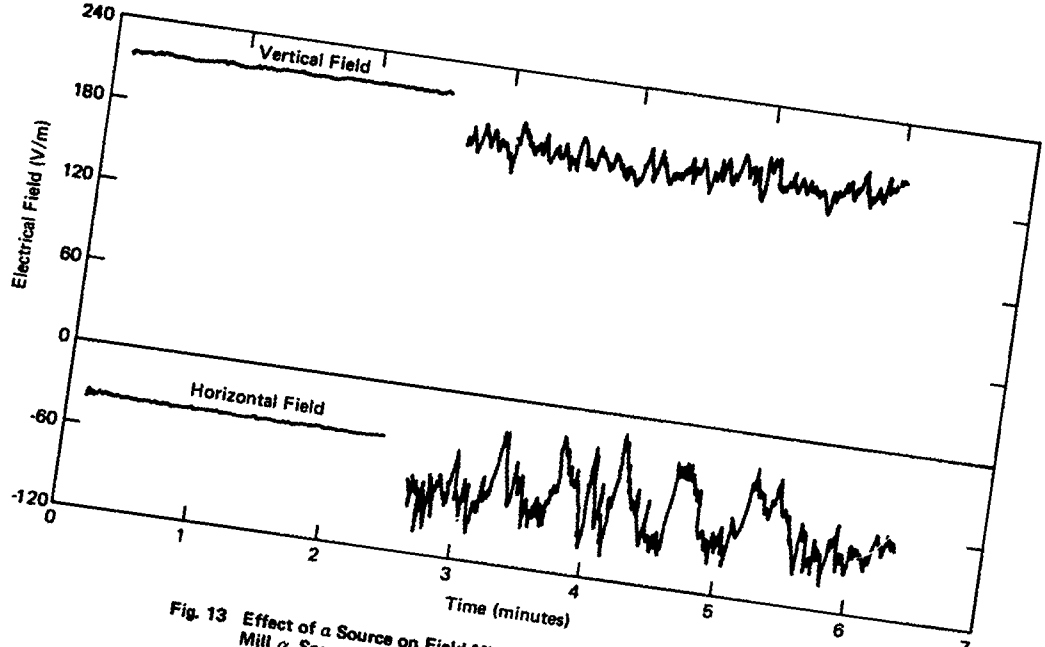

Fig. 13 Effect of α Source on Field Mill; 300 Volts on Capacitor Plates, Field Mill α Source 10 cm from Side

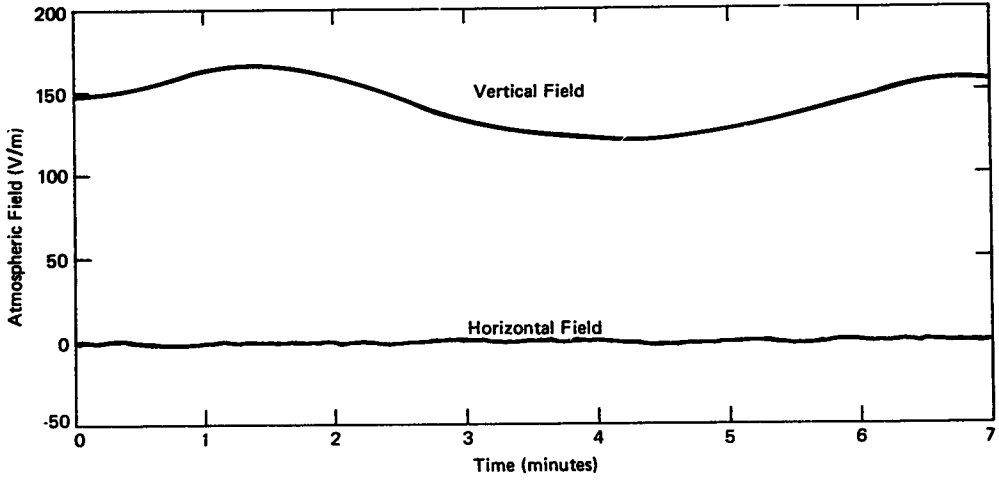

Fig. 14 Vertical and Horizontal Components of Atmospheric Electric Field; Field Mill Measurements

the field mill taken on 7 June 1974 and is to be compared with the high impedance voltmeter reading of the same date shown in Fig. 9. The vertical field shows appreciable changes over periods of several minutes, but there is no measured horizontal field. As pointed out in Section 3, the time response of the field mill to changes in the electric field is faster than 0.5 second, and therefore the smoothness of the above field mill recordings is not the result of instrumental filtering.

From the discussion of the atmospheric field about orographic protrusions in Section 2, it is clear that the fluctuations observed with the high impedance voltmeter coupled to the atmosphere with radioactive sensors pose a serious problem since the fluctuations are of the same order of magnitude as the potential gradients that must be detected. In particular, ground-based measurements of the atmospheric field about orographic protrusions, which are essentially static measurements, will be subject to many inaccuracies and the application of the high impedance voltmeter for terrain avoidance to slowly moving vehicles will be very difficult. However, one might expect that if the air stream moves over the sensor with sufficiently high velocity, the fluctuations will be reduced or eliminated.

The radioactive sensor is surrounded by a region of relatively highly ionized and conducting air. The position of this highly ionized region in the atmosphere may be moved about by local air currents, thus effectively changing the point in space at which the potential is measured. However, it has been well established that, for measurements in the outside atmosphere, the fluctuations can vary greatly from time to time (see Fig. 9). They do not correlate with gross wind velocity. This suggests that the composition of the air is involved and that the nature of the ionic concentration in the high conductivity region may affect the fluctuations.

Three experimental ways to reduce the fluctuations have been attempted: the sensor was ventilated by blowing an air stream across it, the radioactivity of the sensor

was reduced, the effect of source symmetry about the horizontal axis was investigated.

In general, laboratory measurements where the radioactive sensor was placed between capacitor plates have shown that ventilating the sensor with an air stream velocity of 1 to 3 m/s is effective in reducing the fluctuations. Figure 15 shows the effect of ventilating the sensor with an air velocity of 1.5 m/s (about 3 mi/h) originating in a squirrel cage blower 1.85 meters away. For the data in Fig. 15, one sensor is grounded to the meter case and the other placed in the center of the capacitor plates. Thus common mode and differential outputs are redundant, except for a factor of 2. Unfortunately, these results are not reproducible day by day, even in the air-conditioned laboratory. Figure 16 shows data taken under identical conditions 4 days later on a very humid day. This figure reveals that the unventilated sensor signals have greater but slower fluctuations, and that the air velocity must be increased to achieve a degree of smoothing comparable to that shown in Fig. 15. One of the significant results of ventilation most easily observed in the laboratory is that the frequency of fluctuations is always increased by the air flow.

The results of ventilation of the sensor in the outside atmosphere are qualitatively similar to those in the laboratory. In general, ventilation reduces the amplitude and increases the frequency of the fluctuations. However, ventilation tends to be less effective in the atmosphere. On rare occasions it does not help at all, at least for air velocities up to 10 m/s (approximately 22 mi/h). Such an occasion is shown in Fig. 17, where ventilation at 10 m/s does not decrease the fluctuation. These data, like those in the laboratory, were recorded with one sensor grounded, and the potential values are distorted by the air duct in the proximity of the sensor. A simultaneous field mill reading of the vertical field is also shown. The data were recorded on a clear, sunny day with a relative humidity of 43% and very little wind.

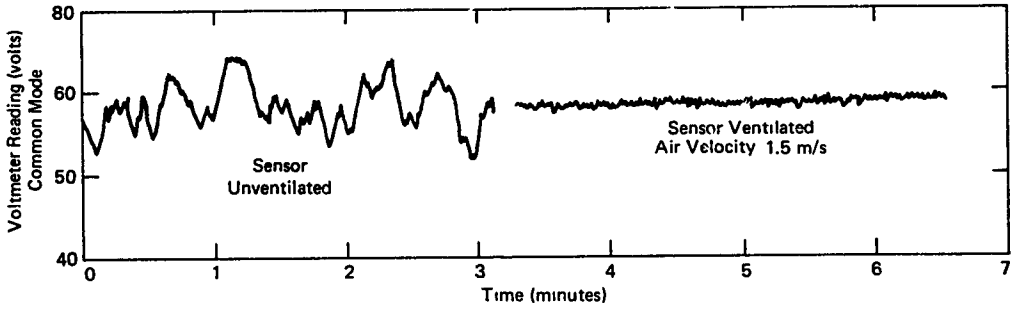

Fig. 15 Effect of Sensor Ventilation on Fluctuation Observed on High-Impedance Voltmeter; Laboratory Measurements, 15 July 1974

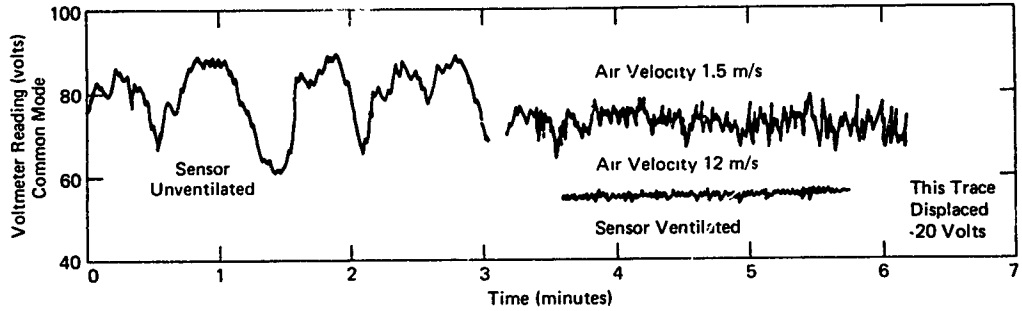

Fig. 16 Effect of Sensor Ventilation on Fluctuations Observed with High-Impedance Voltmeter; Laboratory Measurements, 19 July 1974

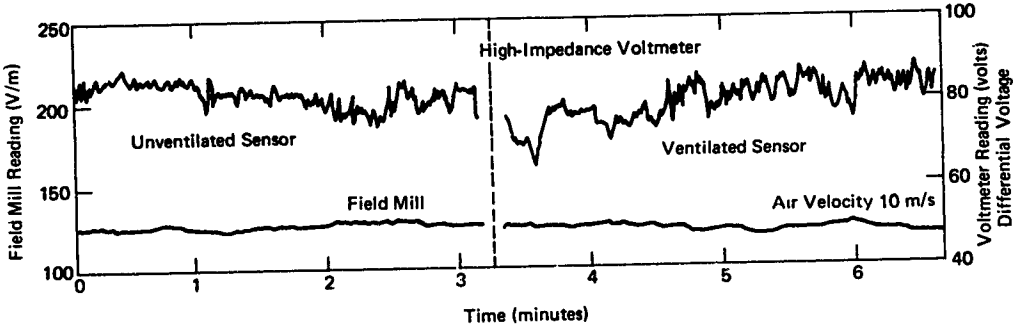

Fig. 17 Effect of Sensor Ventilation on Fluctuations Observed with High-Impedance Voltmeter, Atmospheric Measurements; Results are Atypical

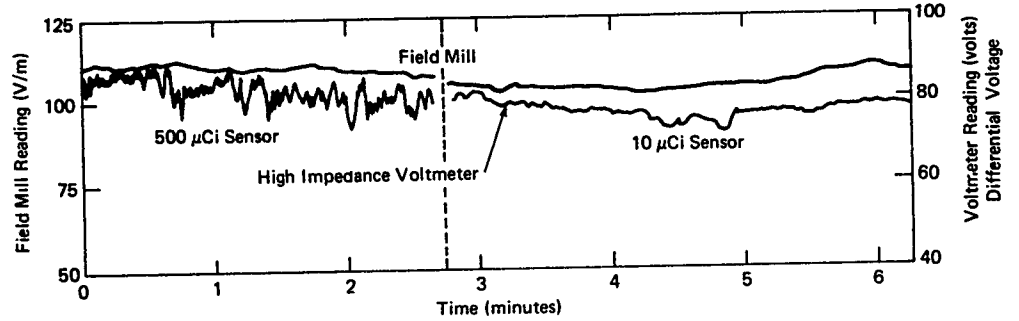

Fig. 18 Effect of Reducing Radioactivity of Sensor, Atmospheric Measurements

The 500 μCi sensor that has been used for the above measurement is much larger than necessary for the high impedance voltmeter. Measurements both in the laboratory and in the outside atmosphere show that the α source strength can be reduced to about 10 μCi without affecting the accuracy of the potential reading or the time response of the instrument. However, a reduction of α source strength below this value affects the accuracy of the potential reading and a source strength of 4 μCi will produce an error of about 5%. The reduction in source strength does decrease the fluctuation, but the reduction is not dramatic until a low enough value of source strength is reached to affect the accuracy of the potential reading. Figure 18 shows the effect of reducing the source strength to 10 μCi. The decrease in fluctuations is significant and the error in the potential reading is negligible. Under those atmospheric conditions (which generally prevail) where ventilation reduces the fluctuations of the 500 μCi sensor, it also reduces the fluctuations of the smaller sensor.

As Ref. 9 points out, there is an inherent error in the potential reading using the sensor shown in Fig. 5. A sensor with cylindrical symmetry about the horizontal axis has been tried on the high impedance voltmeter. The difference in the reading of the atmospheric potential is small (approximately 1 to 2% for a sensor height of 1 meter), and no detectable decrease in fluctuations was observed.

It has been found that a more significant error in the value of the atmospheric potential can be caused by the charging of the fiber glass support rod. In the presence of the normal atmospheric electric field (pointed toward the earth), this rod tends to become negatively charged. This can produce an error of several percent in the potential reading. This charge builds up to a stable value in several minutes when the electric field is applied and requires several minutes to dissipate after the field is removed. If a metal conductor 2 inches long is placed around the fiber glass arm and connected to the guard circuit of the voltmeter (as shown in Fig. 5), this charging effect disappears.

FIELD MEASUREMENTS IN THE NEIGHBORHOOD OF OROGRAPHIC PROTRUSIONS

The ground-level measurements of the atmospheric field in the neighborhood of orographic protrusions were performed using the high impedance voltmeter coupled to the atmosphere with radioactive sensors and mounted on the support stand shown in Fig. 7. From the results given in Section 4, it is obvious that the spurious fluctuations characteristic of this instrument will seriously degrade the accuracy of the measurements, particularly of the horizontal gradient. Further, since such a series of measurements requires a period of an hour or more, it is clear from the results above that significant changes in the vertical field can occur over this period (see Fig. 14). Therefore, during the course of such a measurement, it was necessary to monitor the vertical field with a separate voltmeter remote from the protrusion. The voltmeter readings were recorded by watching the voltmeter with a telescope from distances greater than 30 feet from the instrument.

Measurements were made of the field perturbations in the neighborhood of walls, fences, and small isolated buildings located on the grounds of the APL laboratories in Howard County, Maryland. All of these measurements showed the expected result; that is, as the protrusion was approached on a line parallel to the ground, the atmospheric potential (as measured by the common mode voltage) decreased and the horizontal gradient (as measured by the differential voltage) increased.

An example of these results is shown in Figs. 19 and 20. The high impedance voltmeter with the sensors in a horizontal plane was moved toward a steel mesh fence, 3.2 meters high, at altitudes of 1 and 2 meters. The calculated curves are scaled from the results of Fig. 2. Considering the fluctuations in the meter readings (about ±5 volts) and the time variation of the atmospheric potential (which varied ±20% during the time of this measurement), the agreement of experiment and theory is reasonably good.

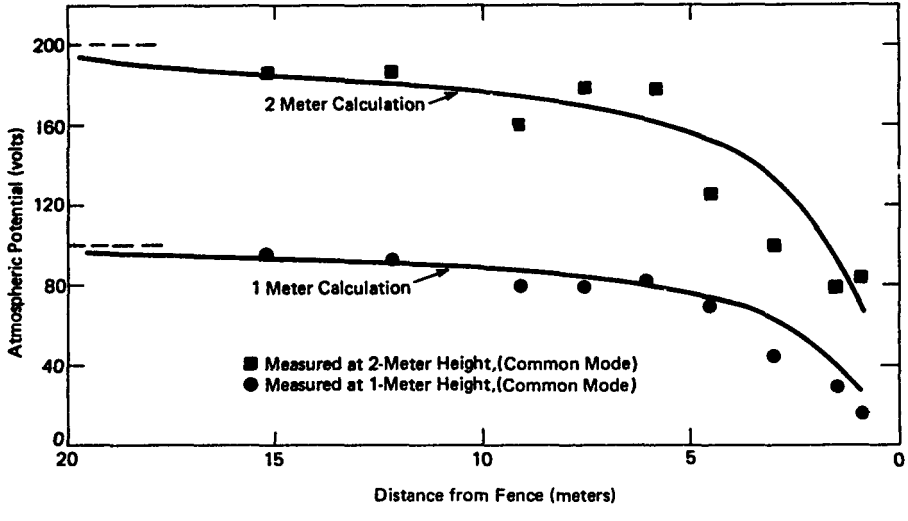

Fig. 19 Atmospheric Potential in Front of 3.2 Meter Steel Fence

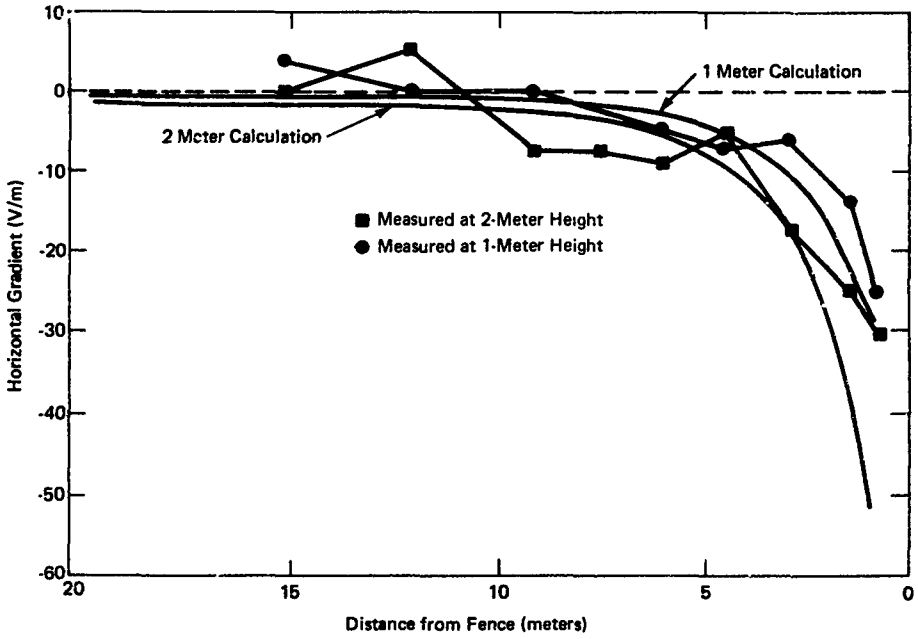

Fig. 20 Horizontal Potential Gradient in Front of 3.2 Meter Steel Fence

From the results shown above, the field meter should be a superior instrument for detecting the perturbations of the atmospheric field caused by orographic protrusions. The field mill that was available was a heavy instrument, requiring 400 cycle AC power, and no field measurements with it were attempted. However, it was mounted on the laboratory roof and its performance as an obstacle detector was compared to that of the high impedance voltmeter. A stepladder covered with a fine conducting mesh was moved toward each instrument. Figure 21 shows the results for the high impedance voltmeter and Fig. 22 for the field mill. The signals are plotted as a function of time for distances of infinity, 5, 4, 3, 2, and 1 meter between the ladder and the instrument. At best, for the voltmeter, the change in the horizontal gradient can be detected 3 meters away; for the field mill, changes in the horizontal gradient of 2 V/m are easily detected at a distance of 5 meters.

The orographic protrusion measurements from the Cessna 337 aircraft were performed by flying north and south along both the eastern and western ridges of South Mountain in western Maryland. As was pointed out in Section 3, for a given flight it was necessary to bias the aircraft frame so that the signal channels to be recorded were not saturated. All the flight data reported here were acquired on flight paths near the top of the ridge and at several hundred feet east or west of the mountain slope. There was no way to determine the position of the aircraft except for the operator's verbal description. These descriptions were tape recorded and synchronized with the instrumentation tape recorder.

An example of the signals recorded in the aircraft, in this case the lower wing sensor differential signal $V_2 - V_4$ flown over level terrain, is shown in Fig. 23. There is no evidence of fast fluctuations on the graph, and the difference signal is correlated with the gyro roll signal. Near the end of this recording the aircraft is entering a right bank. The sense of the signal $V_2 - V_4$ is positive for a right bank.

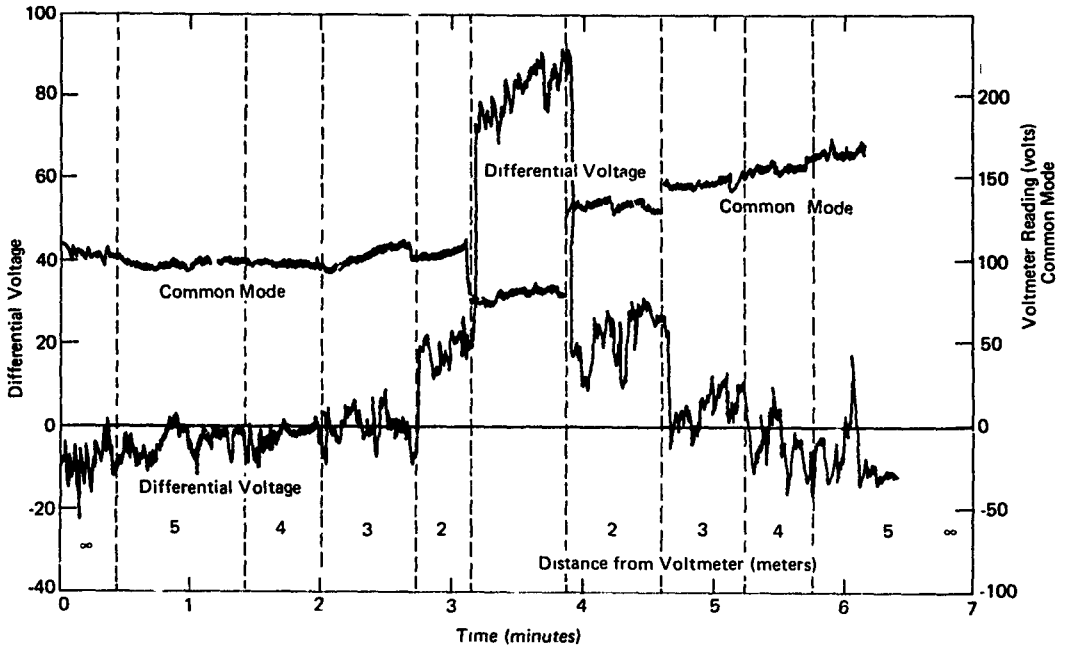

Fig. 21 Common Mode and Differential Voltage versus Time, Measurements Made with High-Impedance Voltmeter at Various Distances in Front of a Ladder 2.4 Meters High

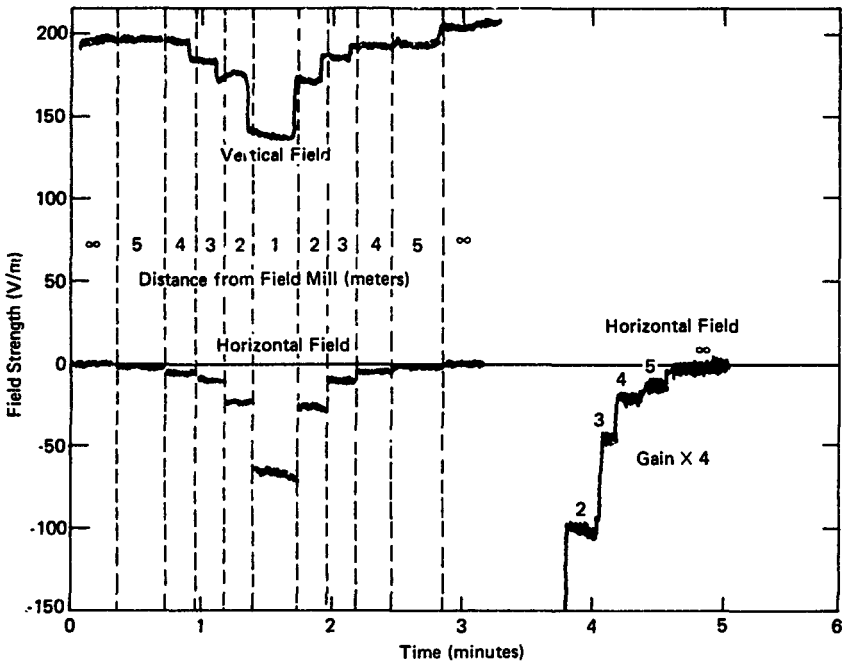

Fig. 22 Vertical and Horizontal Electric Field versus Time, Measurements Made with Field Mill at Various Distances in Front of a Ladder 2.4 Meters High

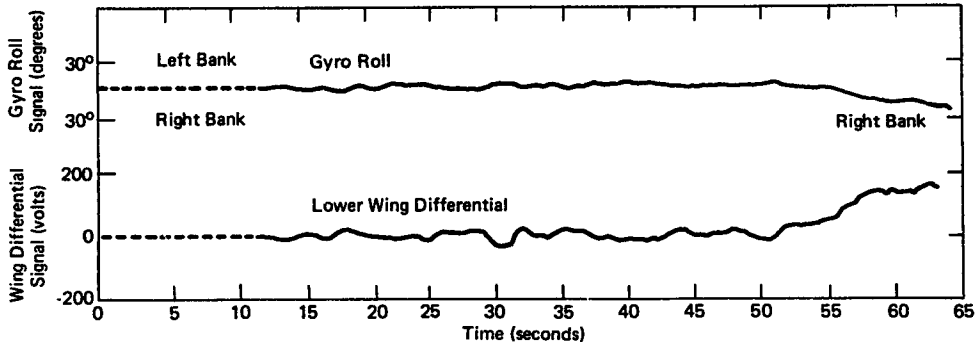

Fig. 23 Lower Wing Differential Signal versus Time, Measurements Made with Cessna 337 Flying over Flat Terrain Level Flight Preceding Right Bank

Figure 24 shows the lower wing sensor differential signal for passes north and south along the east side of South Mountain. Traveling south the right wing is at a lower potential than the left if the field contours are as those of Fig. 3, and therefore the differential signal $V_2 - V_4$ corresponds in sense to that of a left bank. The voltage values given in Figs. 23 and 24 correspond to the difference signal as read by the high impedance voltmeter, but not precisely to the value of the difference in the atmospheric potential between the positions of sensors V_2 and V_4 since the geometric form factors $\alpha_1(\hat{r})$ and $\beta_1(\hat{r})$ of Eq. (22) have not been determined. Thus these data do not give an accurate value of the horizontal gradient. However, for purposes of comparison with the calculations in Fig. 3, it suffices to measure the differential signal $V_2 - V_4$ for a known roll angle over level terrain and to assume that the vertical field does not change significantly during the time of a pass up and down the mountain. It has been well established by Hill and Whyte (Ref. 10) that for roll angles up to 30° the differential signal $V_2 - V_4$ is linear to the accuracy of the measurement. In effect, this establishes for data (such as that in Fig. 24) the slope of the equipotential line, which can then be converted to a horizontal gradient for a nominal value of the vertical gradient of 100 V/m.

Averaging the horizontal gradient for flights north and south along the east and west sides of the mountain, the results are:

Altitude	East side	West side
1300 feet (396 meters)	14.1 V/m	17.5 V/m
2000 feet (610 meters)	8.1 V/m	10.6 V/m

Ref. 10. M. L. Hill and T. R. Whyte, Investigations Related to the Use of Atmospheric Electric Fields for Aircraft and RPV Stabilization, APL/JHU TG 1280 (to be published).

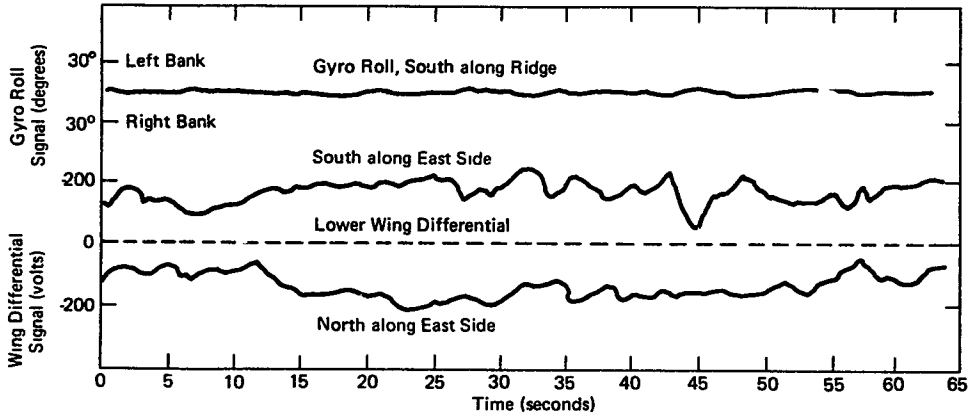

Fig. 24 Lower Wing Differential Signal versus Time; Flights South and North along South Mountain at 1300 Feet

Another flight was made below and off the mountain peak (about 350 meters altitude and several hundred feet from the slope) that yielded the following results when averaged over north and south flight paths on both sides of the mountain:

Sensor position (see Fig. 8)	Horizontal gradient
$V_2 - V_4$	19.5 V/m
$V_1 - V_3$	19.9 V/m
$V_5 - V_6$	16.8 V/m
$V_2 - V_8$	21.3 V/m

Given the uncertainty in the aircraft position, these results are reasonably consistent with those to be expected from the potential contours of Fig. 3.

FLUCTUATIONS IN THE ATMOSPHERIC FIELD

The yearly and daily fluctuations of the atmospheric electric field as discussed in Section 2 and Fig. 14 show that significant short time fluctuations can occur over periods of several minutes. Chapter V of Ref. 3 discusses these short-time fluctuations in some detail, and Refs. 11 and 12 discuss recent investigations of the short-time fluctuations in the fair weather field made without the use of radioactive potential equalizers. The results of Refs. 11 and 12 are in general agreement with the limited amount of data that have been obtained at APL.

Ref. 11. K. Knott and G. Schumann, "Short Period Variation of the Atmospheric Electric Potential Gradient," Arch. Met. Geoph. Biokl., Series A, Vol. 21, 1972, pp. 319-327.

Ref. 12. D. G. Yerg and K. R. Johnson, "Short Period Fluctuations of the Fair Weather Electric Field," J. Geophys. Res., Vol. 79, No. 15, 1974, p. 2177.

Figure 25 is a plot of the vertical and horizontal electric fields recorded from 2:30 PM on 27 June until 9:00 AM on 28 June. The plots were recorded from the roof of an APL building with the field mill mounted 1 meter above the roof and the high impedance voltmeter mounted 3 meters above the roof. The high impedance voltmeter was slower than the one shown in Fig. 4 and the data were recorded on a low precision recorder. The results track well with those of the field mill.

The vertical field has several peaks around midnight which were great enough to overdrive the measuring systems. Also there are field reversals at 1:00 and 4:30 AM. The horizontal field deviated from zero only during these radical changes in the vertical field. These data were recorded on a cloudy night, and the measurements were terminated when rain began to fall about 9:00 AM. No measurable rain (<0.01 inch) fell during the night There is no variation in the meteorological data that matches the fluctuations of the vertical electric field, although it can be observed that violent excursions in the field do correlate with high relative humidity.

A more detailed recording of the time dependence of the vertical and horizontal field changes for a field reversal is shown in Fig. 26.

The high impedance voltmeter station on the flat roof was operated for several months prior to August 1974, and the results can be compared with meteorological data (wind velocity, wind direction, precipitation, humidity, temperature, and barometric pressure) recorded at the same location. The voltmeter recorded both the vertical and horizontal field, but a portion of the horizontal field data are vitiated by a faulty recorder. There is a further question of how accurate the electric field data are during and following periods of precipitation. However, typical results can be summarized below.

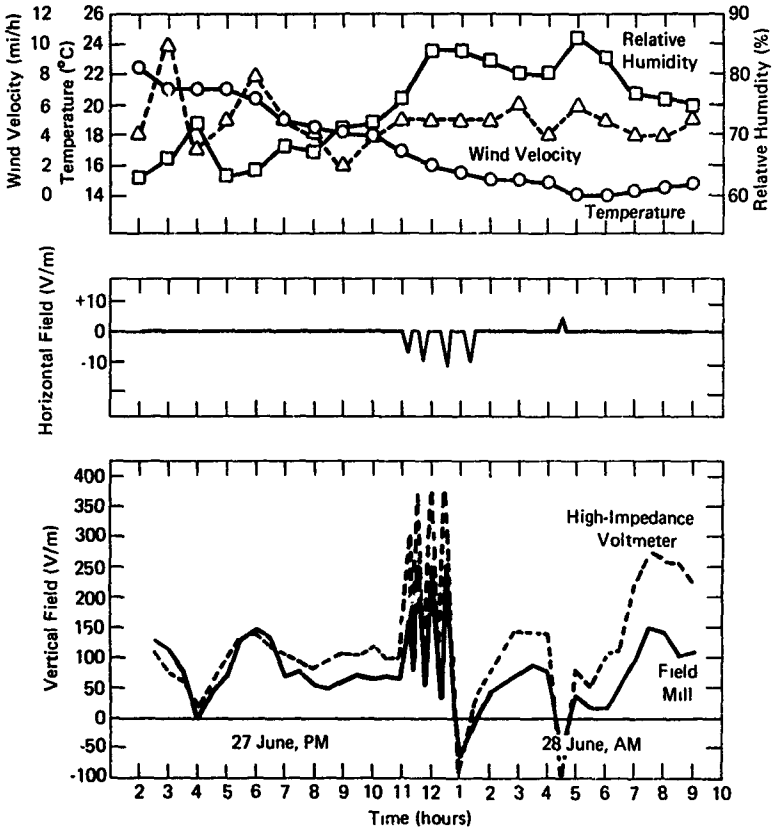

Fig. 25 Atmospheric Electric Field and Meteorological Data versus Time, 27-28 June 1974

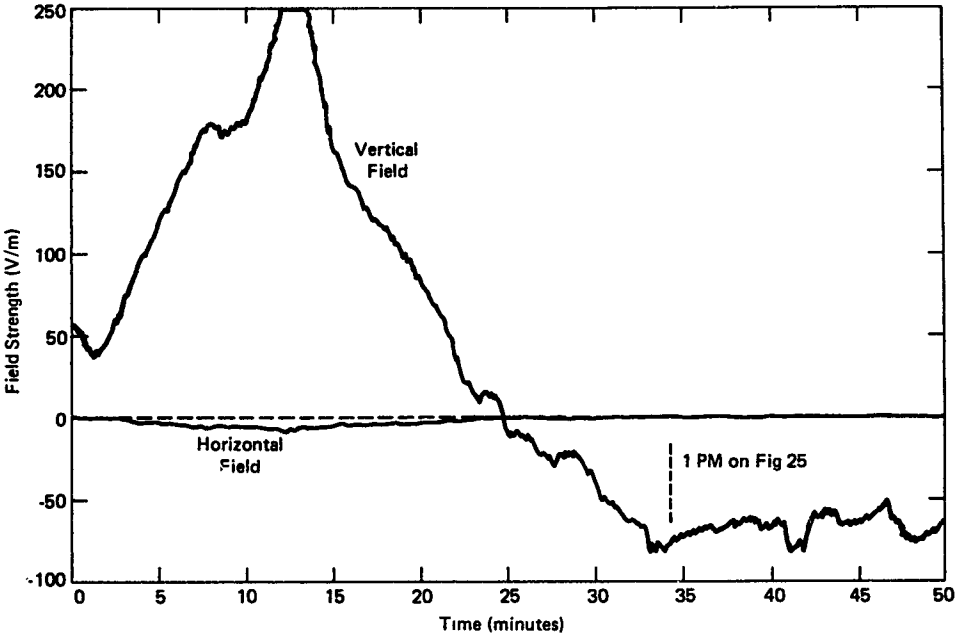

Fig. 26 Field Mill Measurement of Vertical and Horizontal Atmospheric Electric Fields Showing Field Reversal, Measurements Made with Field Mill on Roof at APL. Time: Midnight, 27-28 June 1974

For the period of 15 to 26 March, there were three periods of field reversals. Two of these coincide with periods of precipitation and one with a period of very high humidity. One period of precipitation was not accompanied by a field reversal. In general, the horizontal field is zero except for periods of violent changes in the vertical field. During the period of 16 to 22 July, one field reversal was observed, the only period for which disturbances in the horizontal gradient were noted. The electrical field disturbances occurred near the time of slight precipitation. The results of an unusual night are shown in Fig. 25.

Data recorded and analyzed at APL indicate that when field reversals occur they persist for less than 10% of the total time. Estimates of atmospheric field reversal times made by R. Weiss of APL from American and Russian data (Refs. 13 and 14) indicated that no easy generalization could be made from such information. The data from Pensacola, Florida indicated that for a two-year period field reversals occurred less than 5% of the time. At Norfolk, Virginia the field was reversed for 15% of the time during 1959 and 5.7% of the time during 1960. Russian data showed variations from 7.8 to 20.5%.

The results of Refs. 11 and 12 for the fluctuations of the fair weather are in general agreement with those recorded at APL. At times, appreciable fluctuations are observed over times of several minutes for the vertical

---

Ref. 13. E. M. Trent and R. V. Anderson, "Data from a System of Atmospheric Electricity Stations," U.S. Naval Research Laboratory Report 6162, 20 May 1965.

Ref. 14. "Results of Ground Observations of Atmospheric Electricity," January-December 1970, "USSR Chief Administrations of Hydro-Meteorological Service, Leningrade, 1972.

field; there are periods of hours when the fluctuations do not exceed ±10%. As is pointed out in Ref. 11, fluctuations in the horizontal field are rare. The natural assumption is that these fluctuations are of local origin and are caused by localized variations of charge density or conductivity in space floating over the field sensors (see Refs. 11 and 12). Since changes in the horizontal gradient are not generally observed from ground-based measurements, the fluctuations must be assigned to changes in local conductivity or to space charged clouds at some height above the apparatus. It must be pointed out that the only sensitive evidence for the high degree of accuracy with which the horizontal gradient maintains its zero value over flat terrain is based upon measurements made within a few meters of the earth's surface. This does not preclude the possibility that at altitudes of a hundred meters or so appreciable horizontal gradients might be detected.

5. CONCLUSIONS

The results of the Terrain Avoidance Program can be summarized as follows:

1. The character and magnitude of the atmospheric electric fields about orographic protrusions as computed from Poisson's equation have been experimentally verified for a limited range of parameters.

2. Computations of the fields about orographic protrusions show that both the horizontal and vertical electrical fields contain information of value for terrain avoidance.

3. The solution of Poisson's equation for the atmospheric electric field in the neighborhood of South Mountain shows that the horizontal electric field is about 5 V/m for a ridge 200 meters high as measured from a point 1000 meters from the ridge at an altitude of 100 meters. Since 5 V/m is believed to be a reasonable horizontal field value to detect, and the contour of South Mountain is typical of mountains in the eastern United States, then field disturbances for this class of mountains can be detected at horizontal distances of five times the height for horizontal flight paths lying below the peak of the ridge.

4. Fluctuations in the electric field have been found to be the limiting factor in detecting electric field distortions caused by orographic protrusions. These fluctuations may be real or instrumental. The instrumental errors are not important for field mills nor have they been

shown to be important for high impedance voltmeters coupled to the atmosphere with radioactive sensors for velocities of 80 to 160 mi/h. Experiments indicate that it may be possible, by the proper choice of radioactive source activity and sensor ventilating, to greatly reduce or eliminate the spurious noise that is measured with radioactive sensors in static and low velocity measurements.

5. It seems reasonable to assume that the normal fair weather atmospheric field exists for at least 90% of the time over much of the earth's surface. Perturbations in the horizontal component of the field are very rare near the ground.

Measurements of the atmospheric electric field require specialized equipment and laborious data reduction. The program reported here has been limited in equipment and manpower, and the following problems require further investigation.

1. Can horizontal field gradients of a few volts per meter be reliably measured from aircraft at distances of five scale heights from typical eastern mountains? This problem includes such factors as determining the possible variations in atmospheric conductivity over ranges of thousands of meters, eliminating the effects of wing and tail motion of the aircraft, and using the techniques (which are now available) of computerized data reduction.

2. Verify from an aircraft the predicted changes in the vertical potential gradient near mountains.

3. Determine from aircraft or missiles the most accurate instrumentation for detecting orographic protrusions. The accuracy of the field

mill is well known but further tests should be made with the cheaper high or low impedance voltmeter coupled to the atmosphere with radioactive sensors.

4. Determine for a practical system the logic required to process the simultaneous changes in the vertical and horizontal fields as orographic protrusions are approached.

5. Acquire more information on the fluctuations of the atmospheric field as a function of weather, altitude, and geographic location. The required instrumentation (portable battery powered recorders, sky cameras, and high-altitude platforms) is not presently available.

The final result of such a program would be a recommended list of the instrumentation required for terrain avoidance for a vehicle of specified dynamic performance.

In conclusion, it should be pointed out that the atmospheric electric field may be useful for the following applications:

1. RPV stabilization (this is now well established over a wide range of conditions),

2. Terrain avoidance for low altitude missiles,

3. Long time drift correction in vertical gyros,

4. Helicopter stabilization,

5. High tensior power line detection, and

6. Rotation rate and angular attitude determination for rotating missiles.

REFERENCES

1. M. L. Hill, "Introducing the Electrostatic Autopilot," Astronautics and Aeronautics, 22-31 November 1972.

2. J. A. Chalmers, Atmospheric Electricity, Pergamon Press, New York, N.Y., 1967.

3. H. Israel, Atmospheric Electricity, Vols. I and II, U.S. Department of Commerce, National Technical Information Service, Springfield, Va., 1973.

4. H. Dalezalek, "Discussion of the Fundamental Problems of Atmospheric Electricity," Pure and Applied Geophysics (PAGEOPH), Vol. 100, No. 8, 1972, p. 43.

5. W. A. Hoppel, "Altitude Variations in the Electric Potential Resulting from Orographic Features," Pure and Applied Geophysics (PAGEOPH), Vol. 84, 1971, pp. 57-66.

6. R. L. Konigsberg, "Design of Portable, Solid State, High Input Impedance High Voltage Differential Electrostatic Voltmeter," submitted to Electronic Design, 13 January 1975.

7. H. W. Kasemir, The Cylindrical Field Mill, AD-610485, ECOM, Ft. Monmouth, N.J., 1964.

8. R. Wagner, "Zur Messung des Luftelekrishen Potentialgefälles mittels Kollektoren," Archiv für Meteorologic, Geophysik und Bioklimatologic, Series A, Vol. 8, No. 4, 1955, pp. 427-463.

9. M. L. Hill and W. A. Hoppel, "Effects of Velocity and Other Physical Variables on the Currents and Potentials Generated by Radioactive Collectors in Electric Field Measurements," presented at the Fifth International Conference on Atmospheric Electricity, Garmisch-Partenkirchen, West Germany, 2-7 September 1974.

10. M. H. Hill and T. R. Whyte, Investigation Related to the Use of Atmospheric Electric Fields for Aircraft and RPV Stabilization, APL/JHU TG 1280 (to be published).

11. K. Knott and G. Schumann, "Short Period Variation of the Atmospheric Electric Potential Gradient," Arch. Met. Geoph. Biokl., Series A, Vol. 21, 1972, pp. 319-327.

12. D. G. Yerg and K. R. Johnson, "Short Period Fluctuations of the Fair Weather Electric Field," J. Geophys. Res., Vol. 79, No. 15, 1974, p. 2177.

13. E. M. Trent and R. V. Anderson, Data from a System of Atmospheric Electricity Stations, U.S. Naval Research Laboratory Report 6162, 20 May 1965.

14. "Results of Ground Observation of Atmospheric Electricity, January-December 1970," USSR Chief Administration of Hydro-Meteorological Service, Leningrad, 1972.

APPENDIX A*

ATMOSPHERIC ELECTROSTATIC FIELD NEAR A MOUNTAIN RIDGE

INTRODUCTION

In the absence of various disturbing effects such as a nearby thunderstorm, local air pollution, thermal inversion, and so forth, it is well known that the atmospheric electrical conductivity may be expressed in the form $\sigma = \sigma_0 e^{\beta y}$ where σ_0 and β are constants and y is the altitude. Although there is a wide scatter in the data available for σ_0 and β, a representative set of values is

$$\sigma_o = 4.55 \times 10^{-14} \text{ m-mho}$$

$$\beta = 2.22 \times 10^{-4} \text{ meter}^{-1} \quad . \tag{A1}$$

The electrostatic potential is then determined by the equations

$$\nabla \cdot \vec{J} = 0 \quad , \tag{A2}$$

$$\vec{J} = \sigma \vec{E} \quad , \tag{A3}$$

subject to the applicable boundary condition, where $\vec{J}$ is the electric current density and $\vec{E}$ the field intensity. Equations (A2) and (A3) give the desired differential equation

$$\nabla^2 \varphi + \nabla \ln \sigma \cdot \nabla \varphi = 0 \quad . \tag{A4}$$

*Appendix A was originally published as APL/JHU internal memo QM-74-050 by Kwang Yu, dated 30 April 1974.

Although the ground conductivity is finite, it is known that the ground may be represented by a perfectly conducting boundary.

TWO DIMENSIONAL PROBLEM

We assume that the ground boundary exhibits a translational symmetry in one direction. Taking the x-axis normal to this direction and y-axis vertically upward, the differential equation becomes

$$\frac{\partial^2 \varphi}{\partial x^2} + \frac{\partial^2 \varphi}{\partial y^2} = - \left[\frac{\partial}{\partial y} (\ell n\, \sigma)\right] \cdot \frac{\partial \varphi}{\partial y} \quad . \tag{A5}$$

Before we proceed to solve this problem with a suitable set of boundary conditions, we consider the Laplace equation:

$$\frac{\partial^2 \psi}{\partial x^2} + \frac{\partial^2 \psi}{\partial y^2} = 0 \quad , \tag{A6}$$

subject to the same boundary conditions and a twice differentiable map $F: \psi \rightarrow G = F(\psi)$. Since $\nabla G = F' \nabla \psi$, we have $\nabla^2 G = F' \nabla^2 \psi + F'' (\nabla \psi)^2 = - \left[- \frac{F''}{F'} \nabla \psi \right] \cdot \nabla G$, i.e.,

$$\nabla^2 G + \left[- \frac{F''}{F'} \nabla \psi \right] \cdot \nabla G = 0 \quad . \tag{A7}$$

Comparing Eq. (A7) with Eq. (A4), we note that a mapping F, determined subject to the condition

$$F' = \frac{K}{\sigma}, \quad K = \text{constant} \tag{A8}$$

will yield the solution of the differential Eq. (A5). In particular, for the case of plane symmetry, $\psi \propto y$, and hence

$$\frac{dF}{d\psi} = \text{constant } e^{-\beta y} ,$$

or

$$F = C_1 - C_2 e^{-\beta y} .$$

In general, an exponential transformation of ψ,

$$F = C_1 - C_2 e^{-\beta \psi} = G(x, y) \qquad \text{(A9)}$$

leads to

$$\sigma = \text{constant } e^{+\beta \psi} . \qquad \text{(A10)}$$

Next suppose φ is a solution of Eq. (A4)

$$\nabla^2 \varphi + \nabla \ln \sigma \cdot \nabla \varphi = 0 .$$

Then for any twice differentiable map $F: \varphi \to G = F(\varphi) = G(x, y)$, we have

$$\nabla^2 G = F' \nabla^2 \varphi + F'' (\nabla \varphi)^2$$

$$= F' (-\nabla \ln \sigma \cdot \nabla \varphi) + \left(\frac{F''}{F'} \nabla \varphi\right) \cdot (F' \nabla \varphi)$$

$$= -\nabla G \cdot \nabla \ln \left(\frac{K\sigma}{F'}\right), \quad K = \text{constant} .$$

Thus under the mapping F, φ maps into a solution of another Poisson's equation with σ replaced by $K\sigma/F'$ where K is a constant.

We now consider the effect of boundary condition. Let us examine the behavior of $\varphi = \varphi(x, y)$, satisfying Eq. (4), under the conformal map

$$f: z(=x + iy) \to \zeta = f(z) = \xi + i\eta \ .$$

Denoting

$$\psi(\xi(x, y),\ \eta(x, y)) = \varphi(x, y)$$

$$\tau(\xi(x, y),\ \eta(x, y)) = \sigma(x, y),$$

a simple calculation shows that

$$0 = \nabla^2\varphi + \nabla \ell n\sigma \cdot \nabla\varphi = (\xi_x^2 + \xi_y^2)$$

$$\cdot\ \psi_{\xi\xi} + \psi_{\eta\eta} + (\ell n\tau)_\xi \psi_\xi + (\ell n\tau)_\eta \psi_\eta$$

Thus the conformal mapping $\xi + i\eta = f(x + iy)$ will produce another solution to the Poisson's equation. The boundary condition satisfied by the new solution ψ is determined jointly by that for the solution φ and the conformal mapping. We note that at the transformed point, the conductivity remains the same.

The results established so far show that the order of applying a suitable conformal mapping (to produce the desired boundary effect) and a twice-differentiable map F (to produce the effect of the variable conductivity) may be interchanged in obtaining an approximate solution to a class of two dimensional electrostatic problems.

BOUNDARY CONDITION FOR A MOUNTAIN RIDGE

Suppose ψ is a solution of the Laplace equation with the perfectly conducting plane boundary condition. Then (in suitable units) $\psi = y$, and all the equipotential surfaces are characterized by y = constant. As is well known from

the electrostatics in two dimensions, conformal mapping may be applied to the coordinates x and y to generate the solutions to various boundary value problems. Thus, under the mapping

$$x + iy \rightarrow \zeta = u(x, y) + iv(x, y) \ .$$

The imaginary part v(x, y) gives the solution to the electrostatic potential problem with the boundary given by

$$v(x, y) = 0 \ ,$$

and the equipotential surfaces are then determined by

$$v(x,y) = \text{constant} \ .$$

A procedure related to the above is the Schwarz-Christoffel transformation.* As an example, we will consider the problem of determining the electric potential φ with a perfectly conducting plane boundary with a (grounded) perfectly conducting wall of height "a" standing normal to the x-axis. The transformation we seek is the one characterized by the differential equation

$$\frac{dz}{dw} = \frac{w}{\sqrt{w^2 - a^2}} \ , \ (z = x + iy, \ w = u + iv) \ .$$

Then, in the transformed plane, the problem reduces to:

$$\frac{\partial^2 \psi}{\partial u^2} + \frac{\partial^2 \psi}{\partial v^2} = 0$$

$$\frac{\partial \psi}{\partial u} = 0 \text{ at } u = 0$$

*See, for example, P. M. Morse and H. Feshbach, Methods of Theoretical Physics, Vol. 1, McGraw-Hill, New York, 1953, p. 445.

$$\frac{\partial \psi}{\partial v} = \text{constant, say, 1 at } v = 0$$

$$\psi = 0 \text{ at } v = 0 \ .$$

The differential equation leads to $w = \sqrt{z^2 + a^2}$. As the solution in w-plane is equal to the imaginary part v, the potential in the z plane is given by

$$\psi(x, y) = \text{Im}\left(\sqrt{(x^2 + z^2 - y^2) + i\,2xy}\right) \ ,$$

or

$$\psi(x, y) = \sqrt{\frac{1}{2}\left|\sqrt{(x^2 - y^2 + z^2)^2 + 4x^2y^2} - (x^2 - y^2 + a^2)\right|} \qquad \text{(A11)}$$

The equipotential surfaces are given by ψ = constant.

Explicitly, setting $\psi = \sqrt{c}$, we obtain

$$y(x, c) = \sqrt{\frac{4c^2 + c(x^2 + a^2)}{x^2 + c}} \ . \qquad \text{(A12)}$$

Note that any of the equipotential surface may be taken as the ground boundary provided that φ is corrected by $\sqrt{c}$ to satisfy zero potential condition at the ground.

APPLICATION TO SOUTH MOUNTAIN

Figure A1 is a typical cross section of South Mountain north of Harper's Ferry. This profile can be approximated very closely by the choice c = 0.56 and a correspondence

$$x \rightarrow X = 1270x \text{ (feet)}$$

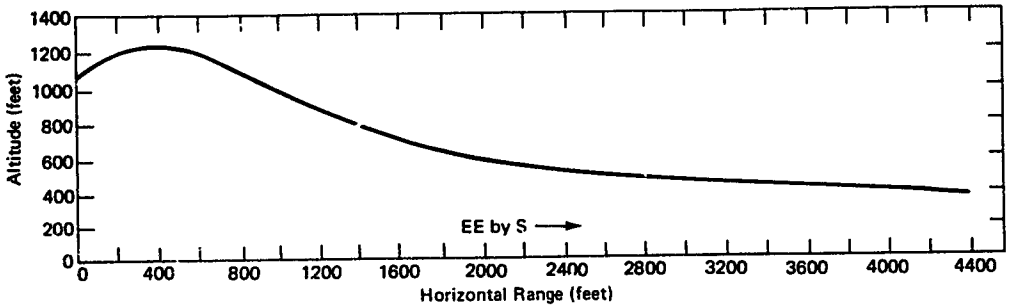

Fig. A1 Profile of South Mountain, 1.2 Miles North of Potomac River

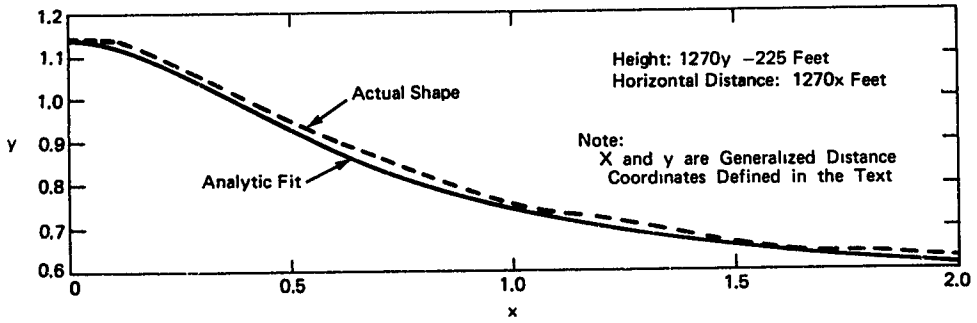

Fig. A2 Comparison of Cross Section of South Mountain with Analytic Approximation, See Fig. A1

$y \rightarrow Y = 1270y - 225$ (feet)

in Eq. (A12). The analytic approximation and the actual cross section as given in Fig. A1 are compared in Fig. A2.

To obtain the solution corresponding to the South Mountain region, we perform the exponential transformation (cf. Eq. (A9)) to Eq. (A11). The constants are so chosen that the electric field intensity at the surface at infinity is 100 V/m. The equipotential surfaces computed are shown in Fig. A3.

In Fig. A4, the surfaces on which the magnitudes of electric field intensity are constant ($|\vec{E}|$ constant) are shown for the South Mountain region. In contrast to the equipotential surfaces of Fig. 3 which are as expected, the surfaces of constant $|\vec{E}|$ at low altitudes exhibit an interesting behavior. In particular, the surface for $|\vec{E}| = 91.1$ V/m contains the saddle point of the function $|\vec{E}(x, y)|$.

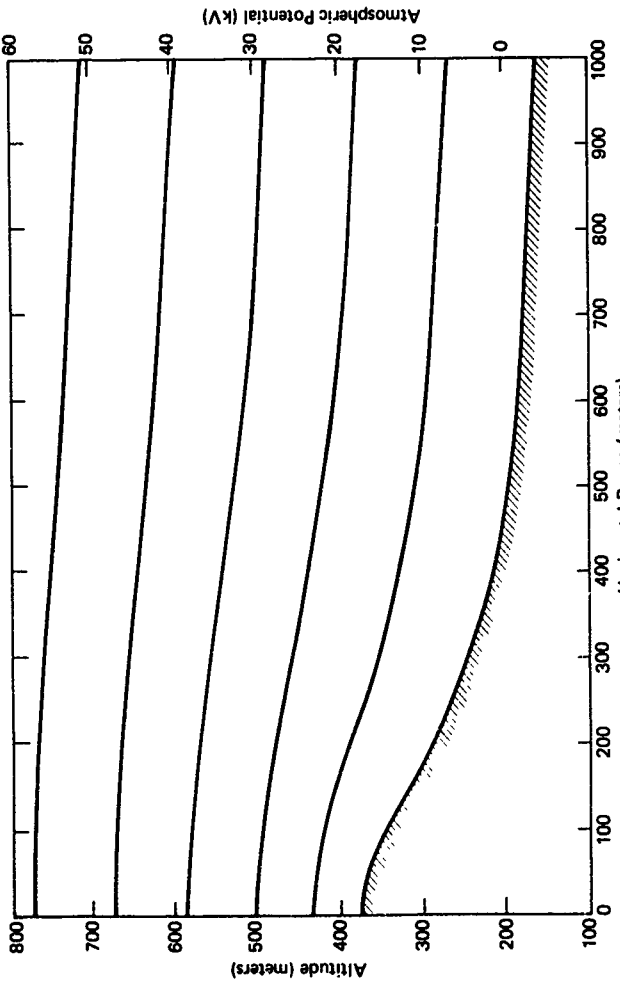

Fig. A3 Equipotential Surfaces, E_o = 100 V/m

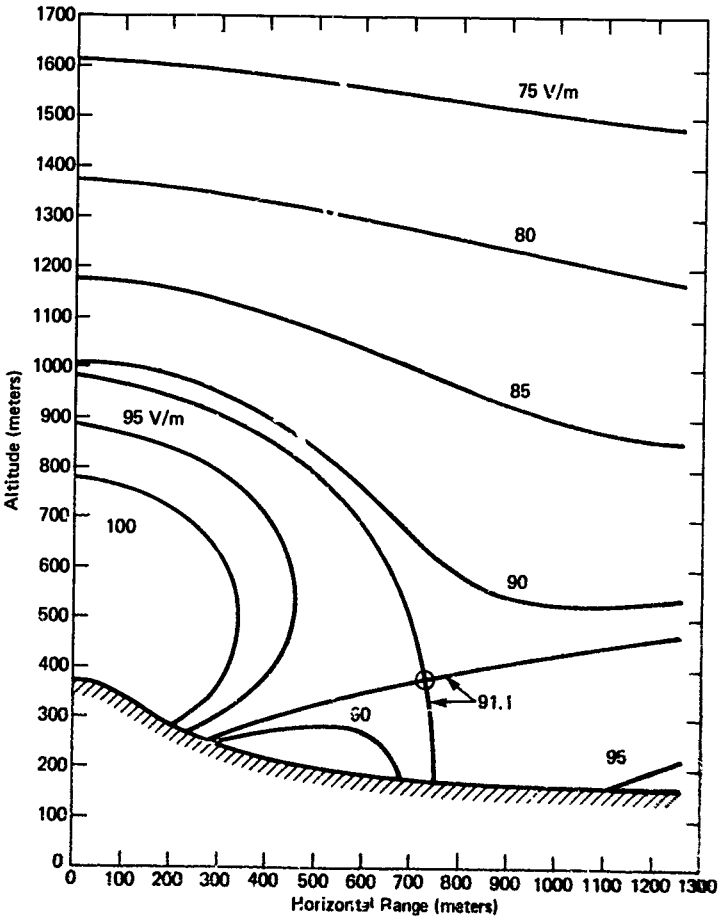

Fig. A4 Surface on which $|\vec{E}|$ = Constant

APPENDIX B*

ELECTROSTATIC POTENTIALS NEAR A PERIODIC SERIES OF MOUNTAIN RIDGES

In a previous memorandum (Appendix A) an analytical technique is considered which may be used to construct solutions to a large class of two dimensional atmospheric electrostatic problems each with an infinitely conducting (not necessarily planar) ground boundary. The method consists of constructing a suitable conformal transformation (including the Schwarz-Christoffel) of a uniform half-space solution to satisfy the ground boundary condition and then performing an exponential mapping to obtain the exponential variation of the atmospheric conductivity.

In this memorandum an application of this method is presented for a class of boundary conditions corresponding to a periodic series of mountain ridges (such as the Appalachian or some parts of the Rocky mountains). We then consider the effects of a localized anomalous air conductivity. Such regions occur as a result of some local radioactivities and/or other localized pollutants.

PERIODIC SERIES OF MOUNTAIN RIDGES

Boundary Condition

The first task is the selection of a suitable mountain profile that is sufficiently simple for computational ease. The profile selected to do this can be obtained from the imaginary part of the conformal mapping

$$z \to f(z) = z - ai\, e^{ibz}, \quad a > 0 \ . \tag{B1}$$

*Appendix B was originally published as API./JHU internal memo QM-74-108 by Kwang Yu, dated 24 July 1974.

i. e.,

$$\eta = y - a \cos bx\, e^{-by} = 0 \quad . \tag{B2}$$

Evidently, in order that this represents the profile of a periodic series of mountain chain the solution $y = y(x)$ must exist and is continuous for all x. This requirement is clearly satisfied if $ab < e^{-1}$*.

Exponential Mapping and the Field Distribution

In order that the exponential mapping $\eta \rightarrow F(e^{\beta\eta})$ generates the solution to the atmospheric electrostatic potential, we put

$$\varphi = F(e^{\beta\eta}) = -\frac{E_o}{\beta}\,(1 - e^{-\beta\eta(x,y)}),\ \beta > 0 \tag{B3}$$

E_o = constant .

$\varphi = 0$ at the ground boundary is represented by $\eta = 0$. The atmospheric conductivity is $\sigma = \sigma_o \exp(+\beta u)$; the small perturbation introduced into the atmospheric conductivity as $e^{-a \cos bx\, e^{by}}$ damps out rapidly as the altitude (y) increases. The constant β then establishes the relation between the dimensionless coordinates (x,y) and the physical coordinates (horizontal range, altitude).

*This may be seen from the function $\lambda(u, v) = ue^{u} - \alpha \cos v = 0$, α = real. The first term has a minimum at $u = -1$, and for all $u > -1$, it is a continuous monotonically increasing function of u. The second term continuously oscillates with the amplitude α. Thus the solution $u = u(v)$ exists only if $|\alpha| < e^{-1}$. As $|\alpha| \rightarrow e^{-1}$, $\left|\frac{du}{dv}\right|_{v = \pi} \rightarrow \infty$.

The electric field is given by

$$\vec{E} = -\nabla\varphi = E_o e^{-\beta\eta}\,\nabla\eta(x,y) \quad ,$$

and the family of equipotential surfaces,

$$\varphi = \text{constant} = -F_o \quad ,$$

is obtained from the equation

$$\eta = \frac{1}{\beta}\,\ell n\left(\frac{E_o}{E_o - F_o\beta}\right) , \quad (>0) \tag{B4}$$

In Fig. B1, a number of equipotential surfaces correspond to several constant values of η.

LOCALIZED ANOMALOUS AIR CONDUCTIVITY

As the starting point, the electrostatic field is considered over a perfectly conducting boundary with the constant conductivity replaced by two uniform conductivity regions. The semicircular inner region has a radius R. In these regions, the potential distribution ψ is given by the imaginary part of the function f

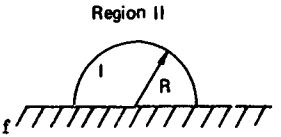

$$f(z) = \begin{cases} f_1(z) = -\dfrac{2\sigma_2}{\sigma_1 + \sigma_2}\, z & |z| < R \\ f_2(z) = -\left(z + \dfrac{\sigma_1 - \sigma_2}{\sigma_1 + \sigma_2} R^2 \dfrac{1}{z}\right) & |z| > R \end{cases} \tag{B5}$$

$$\psi = \begin{cases} \psi_1 = -\dfrac{2\sigma_2}{\sigma_1 + \sigma_2}\, y & x^2 + y^2 \le R \\ \psi_2 = -y + \dfrac{\sigma_1 - \sigma_2}{\sigma_1 + \sigma_2} R^2 \dfrac{y}{x^2 + y^2}, & x^2 + y^2 > R \end{cases} \tag{B6}$$

Several equipotential surfaces for this potential distribution function are shown in Fig. B2 for the case $\sigma_1/\sigma_2 = 2$.

Under the conformal mapping $z \to z - ai\, e^{ibz}$, the conductivity boundary maps into

$$R^2 = x^2 + y^2 + a^2 e^{-2by} + 2a(x \sin by - y \cos bx)\, e^{-by} = \text{constant},$$

and the potential ψ maps into η

$$\psi_1 \to \eta_1 = -\frac{2\sigma_2}{\sigma_1 + \sigma_2}\,(y - a \cos bx\, e^{-by})$$

$$\psi_2 \to \eta_2 = -(y - a \cos bx\, e^{-by}) \left\{ 1 - \frac{\sigma_1 - \sigma_2}{\sigma_1 + \sigma_2} \frac{R^2}{(x + a \sin bx\, e^{-bx})^2 + (y - a \cos bx\, e^{-by})^2} \right\} \tag{B7}$$

We now consider the exponential map

$$\varphi = F(e^{-\beta\eta}) = -\frac{E_o}{\beta}\,(1 - e^{-\beta\eta}) \ . \tag{B8}$$

Note that the equipotential surfaces of φ and η coincide as before. In Fig. B3 several equipotential surfaces are shown which correspond to those given in Fig. B2. In the region where the curves are dotted the potential varies

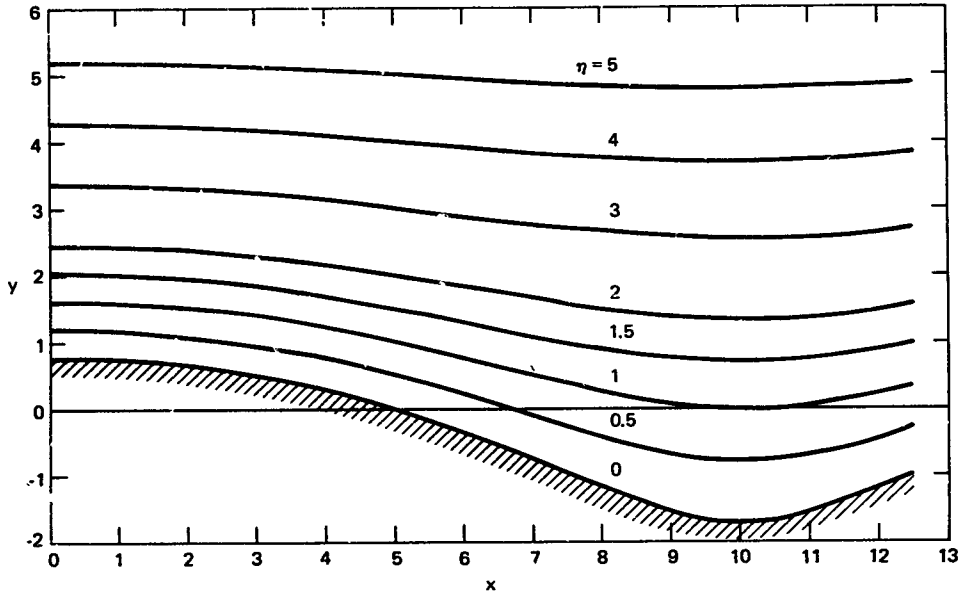

Fig. B1 Equipotential Surfaces in Air over a Periodic Series of Mountain Ridges, $\sigma_1/\sigma_2 = 1$, $\beta = 1$, $a = 1$, $b = \pi/10$

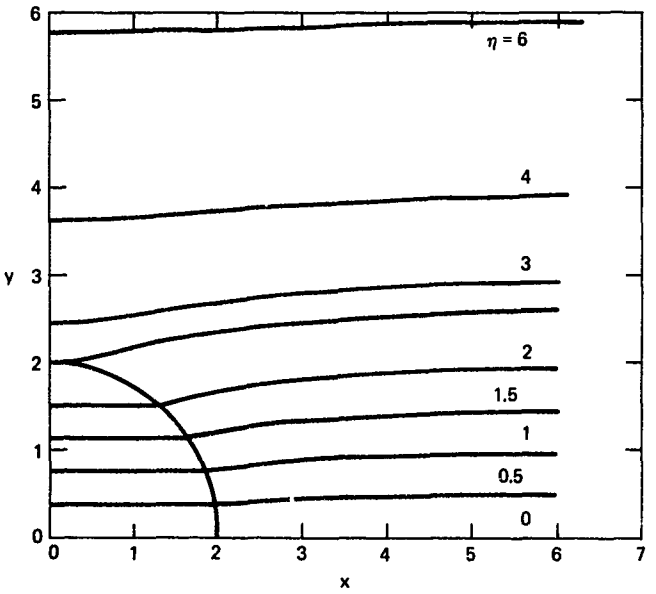

Fig. B2 Equipotential Surfaces with a Semicircular Region of Anomalously High Conductivity, $\sigma_{int}/\sigma_{ext} = 2$

THE JOHNS HOPKINS UNIVERSITY
APPLIED PHYSICS LABORATORY
SILVER SPRING, MARYLAND

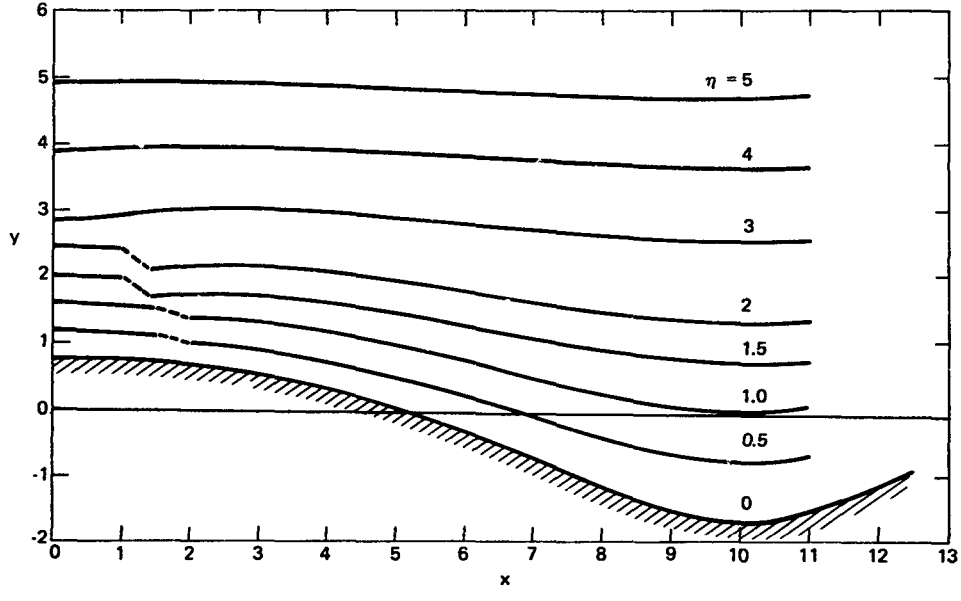

Fig. B3 Equipotential Surfaces over a Periodic Series of Mountain Ridges with a Region of Anomalous Conductivity, $\sigma_1/\sigma_2 = 2$, a = 1, b = π/10, R = 2

rapidly. This is due to the discontinuous conductivity that was used and will be absent if the conductivity is made to vary continuously.

SURFACES OF CONSTANT $|\vec{E}|$

As was done in Ref. B1, the geometry of the surfaces on which $|\vec{E}|$ remains constant is examined. In Fig. B4 three such surfaces are shown for $\beta = 1$ (for ease of computation). This amounts to setting the distance scale so that unit distance corresponds to 4500 meters.

To examine the shapes of the "equi-$|E|$" surfaces with respect to those of equipotential surfaces, the sine* of the angle Θ between $|E|$ = constant surface; the equipotential surface is calculated along the equipotential surfaces corresponding to $\eta = 0, 1, 2, 3,$ and 4 with β set equal to 1. The results are shown in Figs. B5 through B7. To examine the β dependence, for the same set of values for η, sin Θ was computed with $\beta = 1/8$. The results are shown in Figs. B8 through B10. In Figs. B5 to B10, the solid lines show the results corresponding to the presence of anomalous conductivity ($\sigma_1/\sigma_2 = 2$), and the dotted lines to the normal conductivity ($\sigma_1/\sigma_2 = 1$).

As expected, for increasing η the amplitude of $|\sin \Theta|$ decreases, while the maximum amplitude increases as β decreases from 1 to 1/8. The rapid variation near

*The sine of the angle Θ between the two surfaces is computed from

$$\text{Sin } \Theta = \frac{\hat{e}_z \cdot (\vec{E} \times \nabla E^2)}{|E| \cdot |\nabla E^2|} ,$$

where $E^2 = \vec{E} \cdot \vec{E}$ and $\hat{e}_z$ is the right-handed unit vector normal to the xy plane.

Ref. B1. J. A. Stratton, Electromagnetic Theory, McGraw-Hill, 1941.

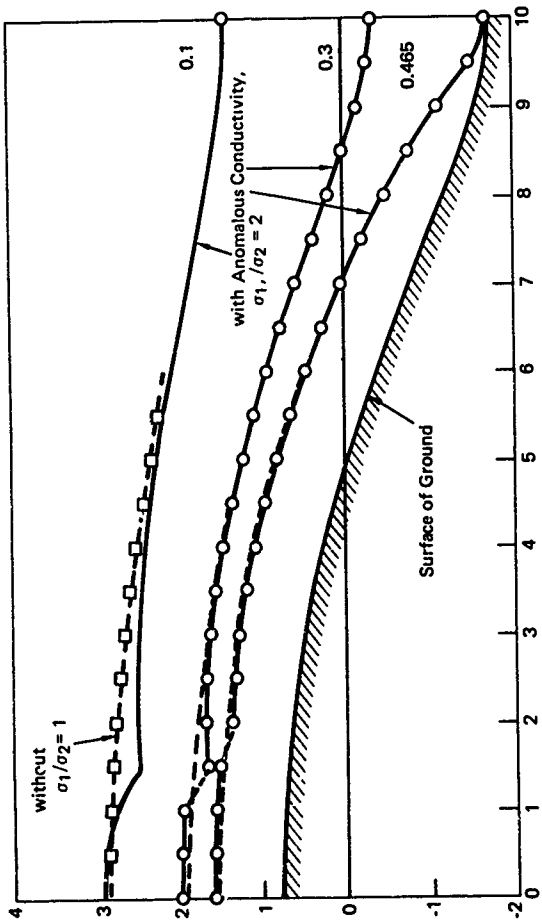

Fig. B4 $|\overline{E}|$ = Constant Surfaces, a = 1, b = $\pi/10$, β = 1, R = 2. Values of E-Field Are with Respect to Dimensionless Distances x(or y)

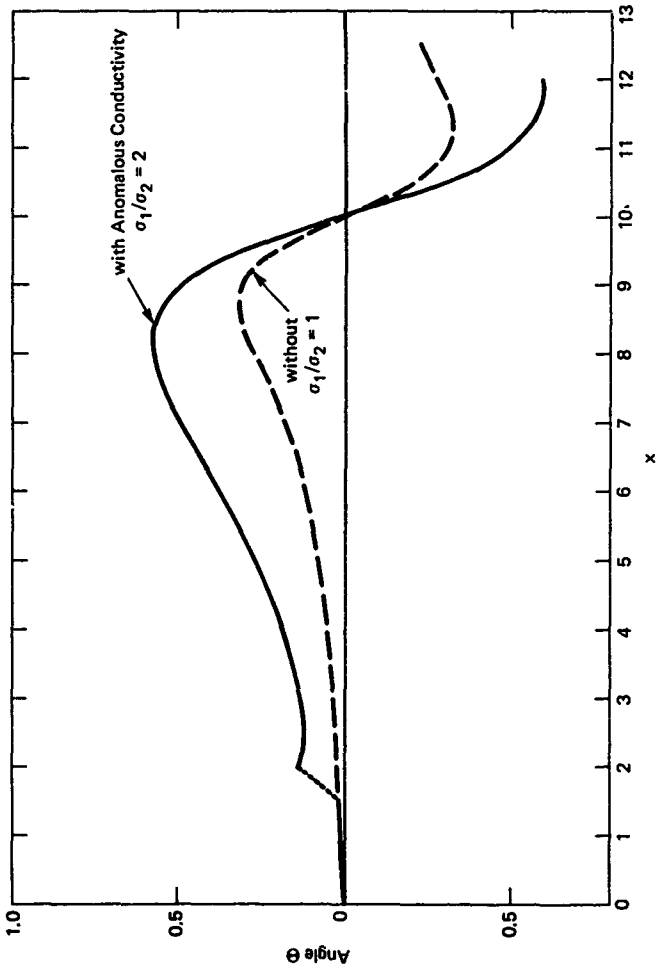

Fig. 35 Angle between $\vec{|E|}$ = Constant Surface and the Equipotential Surface along the Equipotential Surface at $\eta = 0$, a = 1, b = $\pi/10$, $\beta = 1$, R = 2

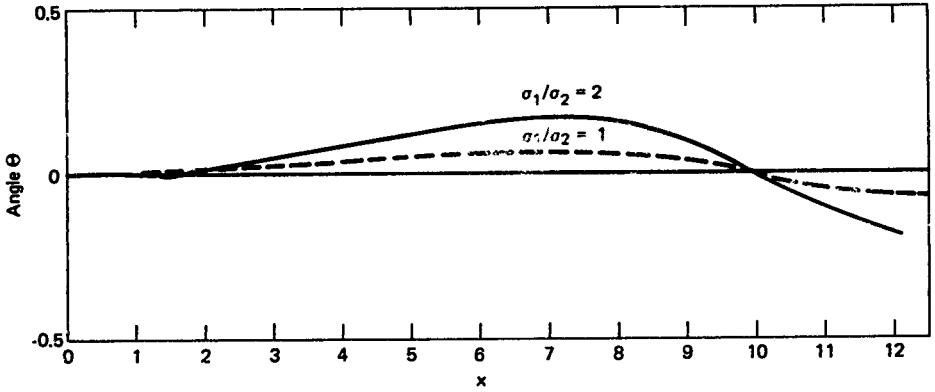

Fig. 86 Angle between $\vec{|E|}$ = Constant Surface and the Equipotential Surface along the Equipotential Surface at $\eta = 2$, a = 1, b = $\pi/10$, $\beta = 1$, R = 2

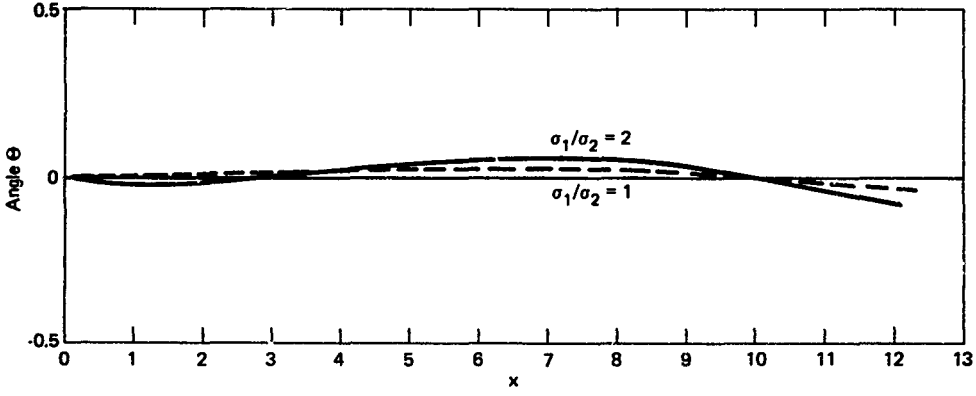

Fig. B7 Angle between $\overrightarrow{IE}$ = Constant Surface and the Equipotential Surface along the Equipotential Surface at $\eta = 4$; a = 1, b = $\pi/10$, $\beta = 1$, R = 2

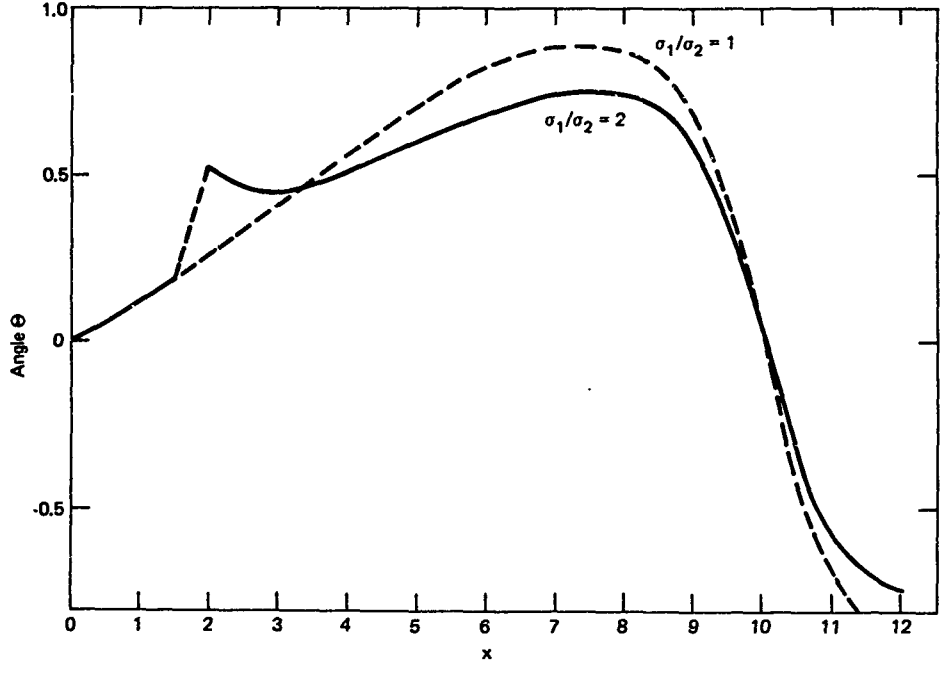

Fig. B8 Angle between $\overrightarrow{|E|}$ = Constant Surface and the Equipotential Surface along the Equipotential Surface at $\eta = 0$, $a = 1$, $b = \pi/10$, $\beta = 1/8$, $R = 2$

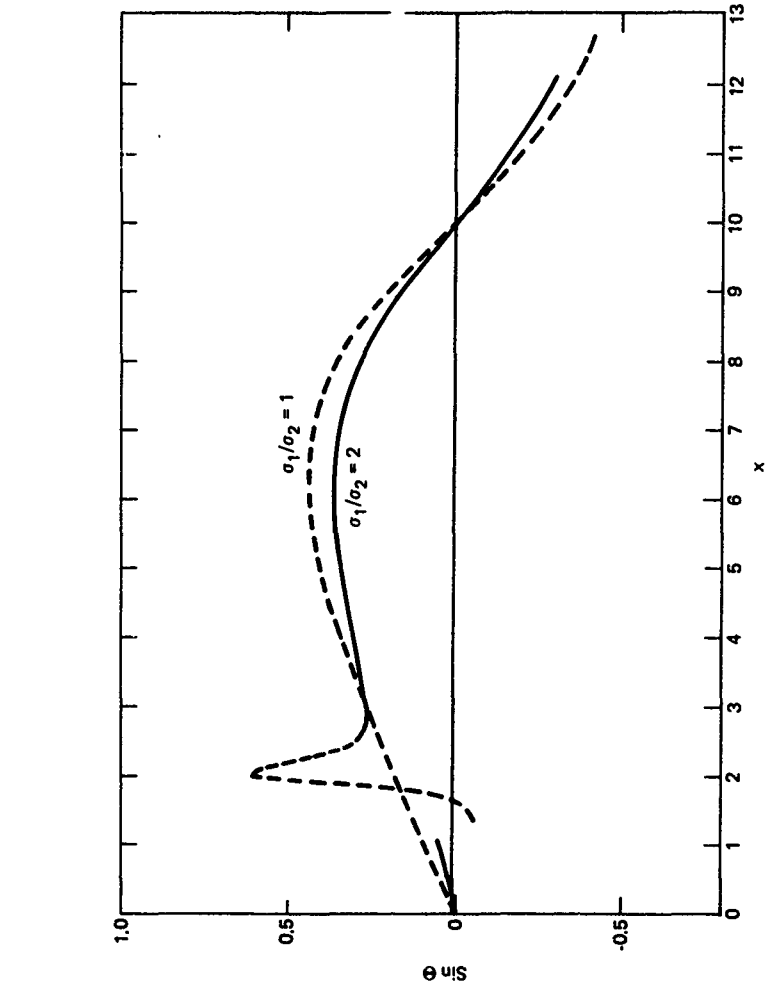

Fig. B9 Angle between $\vec{|E|}$ = Constant Surface and the Equipotential Surface along the Equipotential Surface at $\eta = 2$, $a = 1$, $b = \pi/10$, $\beta = 1/8$, $R = 2$

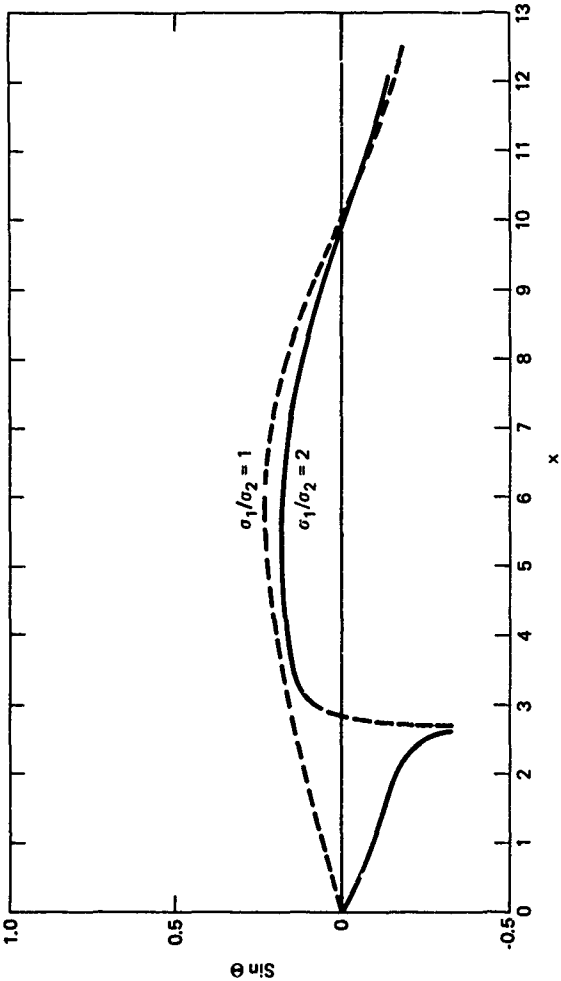

Fig. B10 Angle between $\vec{|E|}$ = Constant Surface and the Equipotential Surface along the Equipotential Surface at $\eta = 4$, $a = 1$, $b = \pi/10$, $\beta = 1/8$, $R = 2$

the conductivity boundary will probably disappear if the conductivity is made to vary smoothly.

To investigate the behavior of $|\vec{E}|$ as a function of altitude in the valley region we put $E^2(x = 10) = \lambda$.

$$\lambda = E^2(x = 10, y, \beta)$$

$$= e^{-2\beta(y + ae^{-by})} (1 - ab\, e^{-by})^2 .$$

At the ground, $\eta(x = 10) = 0 = y + ae^{-by}$, and hence

$$\left(\frac{\partial\lambda}{\partial y}\right)_{\eta = 0} = -2(1 + by_o)\,[\beta(1 + by_o)^2 + b^2 y_o] ,$$

where y_o denotes the ground value of y at x = 0. Setting

$$\beta_c = \frac{b^2 y_o}{(1 + by_o)^2} \approx 0.792, \quad (a = 1,\ b = \pi/10)$$

we have

$$\left(\frac{\partial\lambda}{\partial y}\right)_{x = 10,\ y = y_o} \begin{cases} > 0 \text{ if } \beta < \beta_c \\ = 0 \text{ if } \beta = \beta_c \\ < 0 \text{ if } \beta > \beta_c . \end{cases}$$

In case β is less than β_c, the amplitude of $|\vec{E}|$ is an increasing function of altitude at the ground level in the valley. To see the behavior off the ground we examine

$$\left(\frac{\partial\lambda}{\partial y}\right)_{x = 10,\ y > y_o} = -2e^{-2\beta(y + ae^{-by})} (1 - ab\, e^{-by}) \cdot [\beta(1 - ab\, e^{-by})^2$$

$$-ab^2 e^{-by} .$$

Since $ab < e^{-1}$, the above vanishes only if the square bracket term vanishes. This occurs at $y = y_c$ given by:

$$by_c = \ell n \left[\frac{2\beta ab}{2\beta + b - \sqrt{b^2 + 4b\beta}} \right] .$$

For $y > y_c$, $\left.\frac{\partial \lambda}{\partial y}\right|_{x = 10} < 0$.

Again assuming $\beta > \beta_c$, we consider the behavior of $|E|$ at $x = 10$, $y = y_c$. Evaluating λ_{xx}, λ_{xy}, and λ_{yy}, we have

$$\lambda_{xx}\Big|_{x = 10,\ y = y_c} = 2ab^2 e^{-by_c} e^{-2\beta\eta_c} \left[\beta(1-ab\, e^{-by_c})^2 + b\right] > 0 ,$$

$$\lambda_{xy}\Big|_{x = 10,\ y = y_c} = 0 ,$$

$$\lambda_{yy}\Big|_{x = 10,\ y = y_c} = -2(1-ab\, e^{-by_c})\, e^{-2\beta\eta_c}\, ab^2 e^{-by_c} \left[2\beta(1-ab\, e^{-by_c}) + b\right] < 0 ,$$

where $\eta_c = \eta\big|_{x = 10,\ y = y_c}$,

showing that the point $(x = 10,\ y = y_c)$ is a saddle point.

Values of Parameters for Appalachian Mountains

For the Appalachian mountains in West Virginia, a typical peak-to-peak distance is on the order of 5 to 10 miles (8 to 16 km) with a typical peak-to-valley height in

the range of 1000 to 3000 feet. Taking the height to "wavelength" ratio to be 1/10 we see that the surface corresponding to $\eta = 0.5$, $a = 1$, $b = \pi/10$ may be used to represent the ground boundary. The value of β appropriate for this case is $\beta = 0.111$.

Further Application of the Analytic Technique

Recent measurements of the atmospheric electrostatic field both at APL (near ground) and in the vicinity of South Mountain (airborne measurements) indicate a fluctuation in $E_\perp$ of as much as 10 V/m. This may be due to locally fluctuating regions of anomalous conductivity caused, for example, by some local concentrations of air pollutants.

A two-dimensional analytical analog of this may be constructed by considering a circular (in two-dimensions) region of anomalous conductivity. The solution corresponding to this can then be transformed exponentially, and the field plots (E_x, E_y, $|E|$, etc.) from this can be used to correlate with the experimental data.

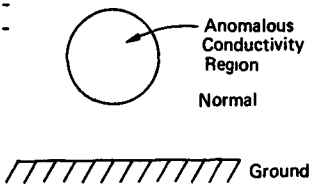

THE JOHNS HOPKINS UNIVERSITY
APPLIED PHYSICS LABORATORY
SILVER SPRING MARYLAND

APPENDIX C*

MEASUREMENT OF ATMOSPHERIC POTENTIAL IN THE NEIGHBORHOOD OF CONDUCTORS OF SIMPLE SHAPE WHICH BEAR A FREE CHARGE

INTRODUCTION

The electrostatic autopilot proposed for RPV's measures the atmospheric potential or a quantity proportional to it, relative to the body of the vehicle, at the position of the sensor. Since aircraft are known to become charged to potentials much higher or lower than their surroundings, it is necessary to examine what effect these potentials have on the attitude sensors.

It would seem clear (at least for shapes that obey certain symmetry properties) that, if the sensors are placed in positions where they are on equipotential surfaces that result from a charge on the vehicle, the difference signals from the sensors will be independent of the potential of the vehicle relative to its surroundings and will accurately measure the atmospheric potential. The following calculations for the sphere and prolate spheroid show that this is true. However, these calculations also indicate that, in practice, it may be difficult to establish these equipotential surfaces for a two-axis system and that the charge on the vehicle can either paralyze or destroy the electronics, even though arranged to only measure the atmospheric potential.

*Appendix C was originally published as APL/JHU internal memo QM-73-167 by C. S. Leffel, Jr., dated 2 November 1973.

CONDUCTING SPHERE IN A UNIFORM ELECTRIC FIELD

For a conducting sphere of radius r_o in a uniform electric field (see Fig. C1)

$$\varphi_o = E_o x = E_o r \cos\theta \,, \tag{C1}$$

the potential field is given by

$$\varphi = Er\cos\theta - \frac{E_o r_o^3}{r^2}\cos\theta + \varphi_s \frac{r_o}{r} \tag{C2}$$

where the first term is the given potential field, the second term is the perturbation term caused by the charges induced on the conductor, and the third term is the potential caused by any free charge on the conductor,

$$\varphi_s = \frac{q}{4\pi\epsilon r_o} \tag{C3}$$

The electric field for $r \geq r_o$ is given by

$$\vec{E} = -\nabla\varphi = \left(E_o\cos\theta - 2E_o\frac{r_o^3}{r^3} + \varphi_s\frac{r_o}{r^2}\right)\hat{r} + \left(E_o\sin\theta - E_o\frac{r_o^3}{r^3}\sin\theta\right)\hat{\theta}. \tag{C4}$$

Along the x axis, the field "augmentation factor," neglecting φ_s, is three.

If potential probes are placed along any line through the center of the sphere, at equal distance $r > r_o$ from the center, and if $V_1 = \varphi(r, \theta) - \varphi_s$ and $V_2 = \varphi(r, \theta + \pi) - \varphi_s$,

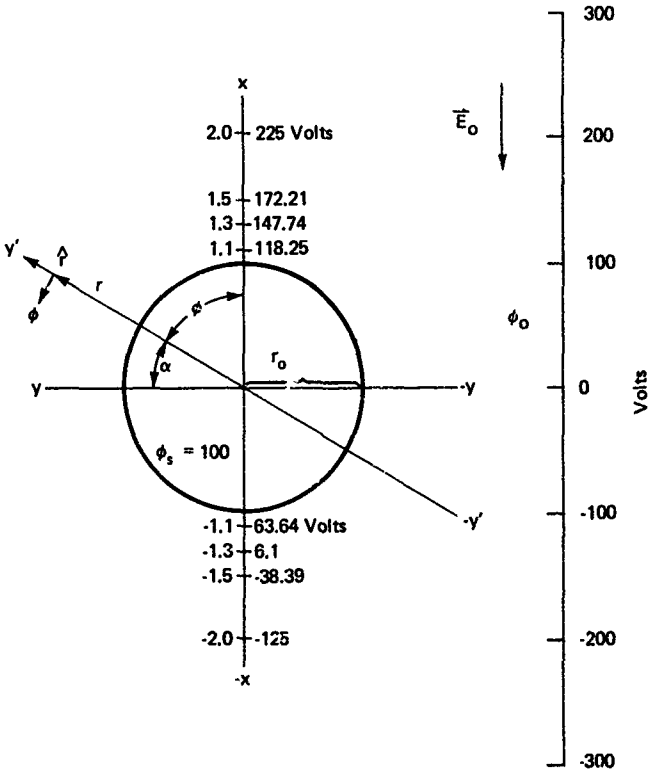

Fig. C1 Conducting Sphere in a Uniform Electric Field

the voltages measured with voltmeters inside the sphere, then

$$\frac{V_1 + V_2}{2} = \varphi_s \left(\frac{r_o}{r} - 1\right) , \qquad \text{(C5)}$$

and the common mode voltage is a measure of the potential of the sphere relative to its surroundings. The difference of V_1 and V_2 is

$$V_1 - V_2 = 2E_o r \cos\theta \left(1 - \frac{r_o^3}{r^3}\right) = 2\varphi_o \left(1 - \frac{r_o^3}{r^3}\right) . \qquad \text{(C6)}$$

Thus $(V_1 - V_2)$ measures φ_o, and the measurement is more sensitive the greater r exceeds r_o. On the other hand, V_1 for example, is given by

$$V_1 = \varphi_o \left(1 - \frac{r_o^3}{r^3}\right) + \varphi_s \left(\frac{r_o}{r} - 1\right) , \qquad \text{(C7)}$$

and if φ_s is great enough and r is great enough, $V_1 \rightarrow -\varphi_s$, which will paralyze or destroy any electronic system.

If the sensors are not symmetrically placed, a change in φ_s can produce a false error signal. For two sensors along the y' axis, fixed to the sphere, placed at distances r_1 and r_2 from the center, then the error signal to maintain the y' axis horizontal is, with $\alpha = (\pi/2) - \theta$.

$$V_1 - V_2 = E_o \sin\alpha \left[r_1 + r_2 - r_o^3 \left(\frac{1}{r_1^2} + \frac{1}{r_2^2}\right)\right] + \varphi_s r_o \left(\frac{1}{r_1} - \frac{1}{r_2}\right) . \qquad \text{(C8)}$$

As long as $\varphi_s = 0$, the error signal will drive the angle α to zero, but if the vehicle becomes charged, then a signal $V_1 - V_2$ will be produced which will drive the y' axis from its horizontal position.

The value of the potential along the x axis for a sphere of 1 meter radius in a field of 100 V/m and with a surface potential of +100 volts is as shown in Fig. C1 and plotted in Fig. C2.

CONDUCTING PROLATE SPHEROID IN A UNIFORM ELECTRIC FIELD

Laplace's equation can be integrated in terms of elementary functions for the prolate spheroid oriented in an electric field as shown in Fig. C3. ξ and ζ define a family of confocal ellipsoidal and hyperboloidal surfaces rotated about the x axis. Here the potential of the field of constant E_o is given by

$$\varphi_o = E_o x = \pm \frac{E_o}{c} \quad (\xi + a^2)(\zeta + b^2) \; . \tag{C9}$$

Assume that the spheroid of constant potential is defined by $\xi = 0$. The potential field caused by free charge on the ellipsoid is given by

$$\varphi_s(\xi) = \frac{q}{8\pi\epsilon} \int_{\xi}^{\infty} \frac{d\xi}{(\xi + b^2)\sqrt{\xi + a^2}} \; ,$$

which when integrated yields

$$\varphi_s(\xi) = \frac{q}{8\pi\epsilon} \; \frac{1}{c} \; \ell n \; \frac{\sqrt{\xi + a^2} + c}{\sqrt{\xi + a^2} - c} \; . \tag{C10}$$

The potential field caused by the charge induced on the spheroid by the $\vec{E}$ field is given by

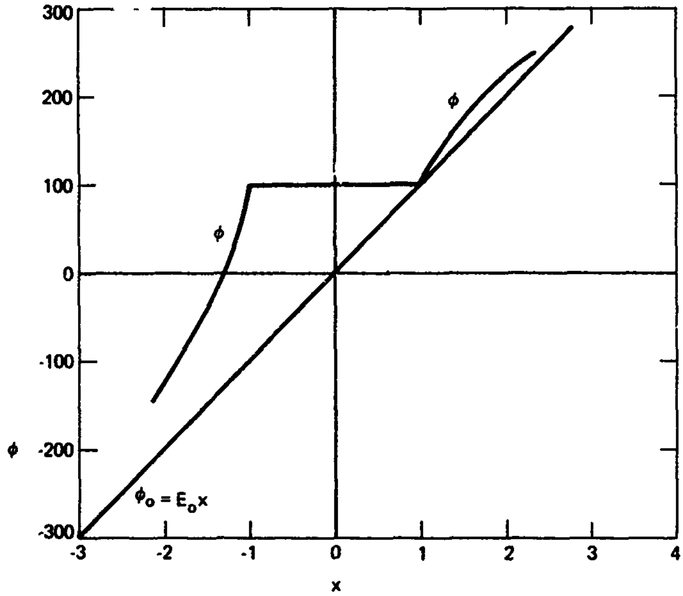

Fig. C2 Potential Field along the x-Axis for a Sphere, ϕ_s = 100 Volts, $\vec{E_0} = -100$ V/m $\hat{x}$

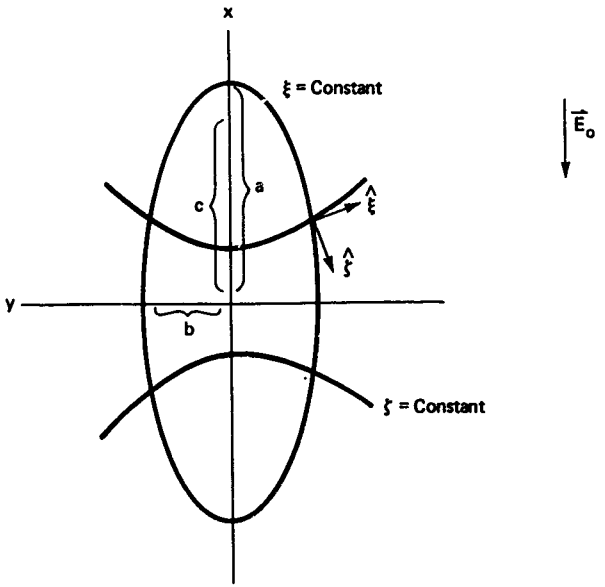

$$\frac{x^2}{a^2+\xi}+\frac{y^2}{b^2+\xi}=1 \qquad \xi > -b^2$$

$$\frac{x^2}{a^2+\zeta}+\frac{y^2}{b^2+\zeta}=1 \qquad -b^2 \zeta > -a^2$$

$$C=\sqrt{a^2-b^2}$$

$$x=\pm\frac{1}{C}\sqrt{(\xi+a^2)(\zeta+a^2)}$$

$$y=\pm\frac{1}{C}\sqrt{-(\xi+b^2)(\zeta+b^2)}$$

Fig. C3 System of Coordinates for Prolate Spheroid

$$\varphi_i(\xi) = \frac{-\varphi_o}{\int_o^\infty \frac{d\xi}{(\xi + a^2)(\xi + b^2)\sqrt{\xi + a^2}}} \int_\xi^\infty \frac{d\xi}{(\xi + a^2)(\xi + b^2)\sqrt{\xi + a^2}} .$$

This integrates to

$$\varphi_i(\xi) = \frac{-\varphi_o}{-\frac{2}{a} + \frac{1}{c} \ell n \frac{a + c}{a - c}} \left(\frac{-2}{\sqrt{\xi + a^2}} + \frac{1}{c} \ell n \frac{\sqrt{\xi + a^2} + c}{\sqrt{\xi + a^2} - c} \right) . \quad \text{(C11)}$$

At $\xi = 0$, $\varphi_i(\xi) = -\varphi_o$ and for the region exterior to the spheroid, the potential is given by

$$\varphi = \varphi_o + \varphi_s(\xi) + \varphi_i(\xi) . \quad \text{(C12)}$$

The electric field in the $\hat{\xi}$ direction is given by

$$E\hat{\xi} = -\frac{1}{h_1} \frac{\partial \varphi}{\partial \xi} = \frac{-2\sqrt{\xi + a^2}\sqrt{\xi + b^2}}{\sqrt{\xi - \zeta}} \frac{\partial \varphi}{\partial \xi}$$

and if we set

$$K = -\frac{2}{a} + \frac{1}{c} \ell n \frac{a + c}{a - c} ,$$

the value of the $\hat{\xi}$ component of the $\vec{E}$ field is

$$E\hat{\xi} = \frac{2\sqrt{\xi + b^2}}{\sqrt{\xi - \zeta}} \left\{ \frac{E_o \sqrt{\zeta + a^2}}{2} - \frac{1}{K} \frac{E_o \sqrt{\zeta + a^2}}{2} \left[\frac{-2}{\sqrt{\xi + a^2}} + \frac{1}{c} \ell n \frac{\sqrt{\xi + a^2} + c}{\sqrt{\xi + a^2} - c} \right] - \frac{E_o}{Kc} \sqrt{(\xi + a^2)(\zeta + a^2)} \left[\frac{1}{\xi + a^2} \right. \right.$$

$$- \frac{1}{(\xi + a^2) - c^2} \Bigg] \Bigg\} . \qquad \text{(C13)}$$

Evaluating Eq. (C13) at $x = a$, $y = 0$ which means $\xi = 0$, $\zeta = -b^2$, the result is

$$E(x = a,\ y = 0) = \frac{-2c^3 E_o}{-2b^2 c + ab^2 \ell n \frac{a + c}{a - c}} \hat{\xi} . \qquad \text{(C14)}$$

If $a \gg b$, the field augmentation factor can be very large at the sharp end of the ellipsoid.

The results of Eq. (C12) are laborious to plot, but except for the lack of spherical symmetry are similar to those of the sphere. The first result to note is that the equipotential surfaces, as given by Eq. (C10) for the free charge on the conducting ellipsoid defined by $\xi = 0$, are simply the ellipsoids defined by $\xi > 0$. Since $\zeta = -b^2$ at the poles $(x, 0)$ and $\zeta = -a^2$ at the equator $(0, y)$, from the equations for x and y given in Fig. C3,

$x = \pm \sqrt{\xi + a^2}$ at the poles

$y = \pm \sqrt{\xi + b^2}$ at the equator.

Thus, from Eq. (C10), if $a = 5$, $b = 1$, and $(q/8\pi\epsilon) = 1$, the following results are obtained:

ξ	$\varphi_s(\xi)$	x	y
0	0.9358	5	1
1	0.7984	5.099	1.414
2	0.7196	5.196	1.032
4	0.6229	5.385	2.236
6	0.5614	5.567	2.645

The equipotential surfaces, which must approach a sphere as ξ increases, lie further from the conducting surface along the y-axis than along the x-axis.

The values of the potential near the ellipsoid along the x axis are plotted on Fig. C4 and along the y axis on Fig. C5, for a = 5 meters, b = 1 meter, E_o = 100 V/m and $\varphi_s(\xi = 0) = 93.5$ volts. Compared to the sphere, the rate of change of potential is much faster along the x axis and slower along the y axis. In either case, at distances far enough from the origin, the value of φ asymptotically approaches φ_o.

If sensors are mounted along a line through the center of the ellipsoid and if V is measured relative to $\varphi_s(\xi = 0)$, and if $V_1 = V(x, y)$, $V_2 = V(-x, -y)$, then since $\varphi_o(x, y) = -\varphi_o(-x, -y)$, then from Eq. (C12)

$$V_1 = \varphi_o + \varphi_s(\xi) + \varphi_i(\xi) - \varphi_s(\xi = 0) \ .$$

$V_2 = -\varphi_o + \varphi_s(\xi) - \varphi_i(\xi) - \varphi_s(\xi = 0)$, and again we have the results

$$\frac{V_1 + V_2}{2} = \varphi_s(\xi) - \varphi_s(\xi = 0) \qquad \text{(C15)}$$

$$V_1 - V_2 = 2[\varphi_o(\xi, \zeta) + \varphi_i(\xi, \zeta)] \ . \qquad \text{(C16)}$$

From Eq. C11, it is observed that $\varphi_i(\xi, \zeta)$ can be written as

$$\varphi_i(\xi, \zeta) = -\varphi_o(\xi, \zeta)\gamma(\xi) \ .$$

Thus Eq. (C16) can be written as

$$V_1 - V_2 = 2\varphi_o(\xi, \zeta)[1 - \gamma(\xi)] \ , \qquad \text{(C17)}$$

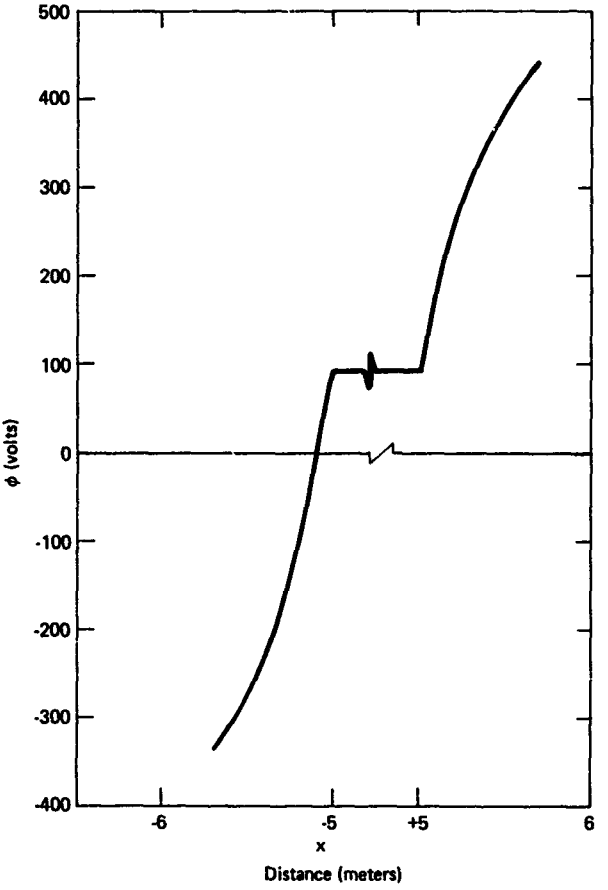

Fig. C4 Potential along Axis of Prolate Spheroid, $E_o = -100\ V/m\ \hat{x}$, $\phi_s = 93.5$ Volts, a = 5 Meters, b = 1 Meter

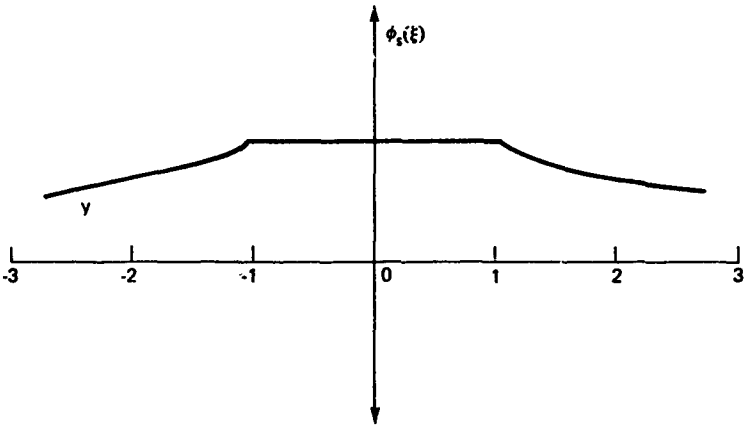

Fig. C5 $\hat{\phi}_s(\xi)$ versus y for ϕ_s Equals 93.5 Volts; Oblate Spheroid, $\vec{E}_o = E_o \hat{x}$

where $\gamma(\xi)$ is 1 for $\xi = 0$. Equations (C15) and (C17) are identical in form to Eqs. (C5) and (C6) for the sphere. Thus $\varphi_s(\xi)$, caused by the self charge and φ_o, caused by the external field can be measured if the geometrical factors are known.

CONCLUSIONS

1. Since the potential field caused by free charge on the surface of the vehicle is fixed in the coordinate systems of the vehicle itself, it can always be measured by an equation of the form of Eq. (C15), no matter how complicated, provided the sensors are on equipotential surfaces. Further, for the difference voltages, the effect of the free charge potential will always cancel out.

However, in the case of an actual RPV, the equipotential surfaces caused by free charge may be very difficult to determine. For the roll axis, sensors on the wing tips will by the symmetry of the vehicle body easily be placed on or nearly on an equipotential surface caused by free charge. But the problem is much more difficult for the pitch axis; if the fore and aft sensors are not on equipotential surfaces, an accumulation of charge on the vehicle body will produce a climb or dive. To find the free charge equipotential surfaces by analysis for a realistic vehicle shape seems a formidable task. An experimental approach in which the vehicle is suspended and the sensor positions adjusted for zero difference signals as voltages are applied to the vehicle skin may be more promising. However, the problem is complicated by the ground plane effects (image charges) which have not been considered here, and which may be important when an RPV is charged under laboratory conditions.

Since it is necessary, in order to detect the atmospheric potential, that the sensors be placed outside the free charge equipotential surface of the vehicle, it is always possible that the vehicle can become charged to a potential that will saturate any realistic measuring circuit.

2. The above calculations for the prolate spheroid are not adequate for the case in which the major axis of the spheroid is displaced from the direction of the atmospheric field. That is to say, the values calculated for φ_o and γ will no longer be correct. However, because of the symmetry of the spheroid the form Eq. (C17) will still be applicable. However, even in the case of lack of symmetry, it would appear that the error signal $V_1 - V_2$ will always be such to move the body so that the sensors lie in atmospheric equipotential planes. For in general, the difference voltage will be of the form:

$$V_2 - V_1 = \varphi_{o1}(1 - \gamma_1) + \varphi_{o2}(1 - \gamma_2) \ ,$$

and since $\gamma < 1$ and $\varphi_{o1} = \varphi_{o2} = 0$ when the sensors are in atmospheric equipotential planes, the error signal can be coupled to the controls so that $V_2 - V_1$ is driven to zero.

ACKNOWLEDGMENTS

The work contained in this report was supported by the Defense Advanced Research Projects Agency (Order TTO AO 2561) and supervised by the Applied Physics Laboratory The Johns Hopkins University Advanced Research Projects Office, Dr. A. M. Stone, Director.

The authors acknowledge the assistance of Mr. T. R. Whyte who conducted the measurements from the instrumented aircraft, Mr. R. Konigsberg who designed the high impedance voltmeters used on both the aircraft and ground-based measurement programs, and Mr. C. Keller who assisted in the instrumentation and performance of the ground-based measurements. The computer and analytic solutions of Poisson's equations were performed by Dr. R. Weiss and Mr. K. Yu, respectively.

In the interest of economy of effort and apparatus, the Terrain Avoidance Program has been coordinated with the Remotely Piloted Vehicle Electrostatic Stabilization Program conducted by APL and supported by the U. S. Army through ECOM, Fort Monmouth, New Jersey.

INITIAL DISTRIBUTION EXTERNAL TO THE APPLIED PHYSICS LABORATORY*

The work reported in TG 1271 was done under Navy Contract N00017-72-C-4401. The work is related to Task QOYO which is supported by the Defense Advanced Research Projects Agency.

ORGANIZATION	LOCATION	ATTENTION	No. of Copies
DEPARTMENT OF DEFENSE			
Dir. ARPA	Arlington, Va.	TIO	1
Advanced Research Projects Agency	Arlington, Va.	A. J. Tachmindji	1
		K. Kresa	1
		R. Moore	1
		Capt. M. Byrd	1
		R. M. Chapman	1
		K. Perko	1
		L. Strom	1
		LTC. P. Worch	1
		C. Hartsell	1
		E. H. Willis	1
		F. W. Niedenfuhr	1
		F. Koether	1
DDC	Alexandria, Va.		12
Department of the Navy			
NAVSEASYSCOM	Washington, D.C.	SEA-09G3	2
NAVAIRSYSCOM	Washington, D.C.	Capt. W. Locke	1
		C. Tross	1
		Capt. F. Hill	1
		AIR-53664	2
NAVPRO	Silver Spring, Md.		1
NRL	Washington, D.C.	L. Ruhnke	1
NSWC	Dahlgren, Va.	Chief Scientist	1
ONR	Washington, D.C.	J. Hughes	1
Department of the Air Force			
Headquarters, USAF	Washington, D.C.	AFRDD	1
Department of the Army			
Ass't. Secretary of the Army (R&D)	Washington, D.C.	Ass't. for Research	1
		Ass't. for Electronics	1
Army Material Command	Alexandria, Va.	AMORD-O	1
Army Missile Command	Redstone Arsenal, Ala.	AMSMI-RDD	1
Army Intelligence School	Ft. Huachuca, Ariz.	ATSIT-CTD-MS, (COL. S. Arculis)	1
Army Field Artillery School	Ft. Sill, Okla.	RPV Task Force (COL. Kretzer)	1
Army Aviation Systems Command	St. Louis, Mo.	AMSAV-O (LTC. D. Powers)	1
Army Research Office - Durham	Durham, N.C.	A. Dodd	1
Chief of Research and Development	Washington, D.C.	DARD-DDS-S (MAJ. J. Clifton)	1
Army Air Mobility R&D Laboratory	Moffett Field, Cal.	T. Gossett	1
Eustice Directorate USAAMRDL	Ft. Eustis, Va.	SAVDL-EU-SYA (S. B. Poteate)	1
Army Electronics Command	Ft. Monmouth, N.J.	AMSEL-NV-D	1
		AMSEL-WL-D	1
		AMSEL-NL-D	1
		AMSEL-TL-D	1
		AMSEL-VL-D	1
		AMSEL-BL-D	1
		AMSEL-CT-A	1

Requests for copies of this report from DoD activities and contractors should be directed to DDC, Cameron Station, Alexandria, Virginia 22314 using DDC Form 1 and, if necessary, DDC Form 56

*Initial distribution of this document within the Applied Physics Laboratory has been made in accordance with a list on file in the APL Technical Publications Group.

Preceding page blank

INITIAL DISTRIBUTION EXTERNAL TO THE APPLIED PHYSICS LABORATORY*

TG 1271

ORGANIZATION	LOCATION	ATTENTION	No of Copies
Department of the Army (cont'd)			
Army Electronics Command (cont'd)	Fort Monmouth, N.J.	AMSEL-SI-CB	1
		AMSEL-MA-MP	1
		AMSEL-MS-TT	1
		AMSEL-GG-TD	1
		CSCS-FM	1
		AMSEL-EN	1
		AMSEL-PA	1
		AMCPM-TDS-SE	1
		USMC-I ND	1
CONTRACTORS			
Aerospace Corp.	Los Angeles, Cal.	Library	1
Analytic Services, Inc.	Falls Church, Va.	Library	1
Battelle Memorial Inst.	Columbus, Ohio	R. Kohn Attn: STOIAC	1
General Research Corp.	McLean, Va.	Document Control	1
General Research C orp.	Santa Barbara, Cal.	Library	1
Institute for Defense Analyses	Arlington, Va.	R. Swanson	1
MIT/LL	Lexington, Mass.	Library	1
MITRE Corp.	Bedford, Mass.	Document Control Ctr.	1
Rand Corp.	Santa Monica, Cal.	Library	1
Riverside Research Inst.	Arlington, Va.	J. L. Torres	1
Riverside Research Inst.	New York, N.Y.	H. Cressman	1
Stanford Research Inst.	Menlo Park, Cal.	Document Service	1
	NOTICE OF AVAILABILITY SENT TO THE FOLLOWING:		
DEPARTMENT OF DEFENSE			
DDR&E	Washington, D.C.	Capt. R. C. Avrit	
Dir , WSEG	Washington, D.C.		
Tactical Technology Info. Analysis Ctr.	Columbus, Ohio	Nancy Hall	
Information Analysis Ctr., CPIA	Silver Spring, Md.		
Department of the Navy			
Department Offices			
CNO	Washington, D.C.	OP-60	
NAVSEASYSCOM	Washington, D.C.	SEA-00	
		SEA-03	
		SEA-03B	
		SEA-03C	
		SEA-03131	
		SEA-03134	
		SEA-032	
		SEA-0324	
		SEA-033	
		SEA-0331	
		SEA-034	
		SEA-035	
		SEA-0462	
		SEA-06G	
		SEA-6512	
		SEA-652	
		SEA-653	

*Initial distribution of this document within the Applied Physics Laboratory has been made in accordance with a list on file in the APL Technical Publications Group.

INITIAL DISTRIBUTION EXTERNAL TO THE APPLIED PHYSICS LABORATORY*

TG 1271

ORGANIZATION	LOCATION	ATTENTION	No. of Copies
Department of the Navy (cont'd)			
Department Offices (cont'd)			
NAVSEASYSCOM (cont'd)		SEA-654	
		SEA-6541	
		SEA-6542	
		SEA-6543	
		PMS 304-20	
		PMS 404-032	
		PMS-405	
CNM	Washington, D.C.	NMAT-03	
		NMAT-03L	
		NMAT-03L1 (Capt. Keach)	
		NMAT-032	
NAVAIRSYSCOM	Washington, D.C.	AIR-00	
		AIR-03	
		AIR-03B	
		AIR-03C	
		AIR-330	
		AIR-5108	
		AIR-520A	
		AIR-520C	
		AIR-5203	
		AIR-535	
		AIR-50174	
Strategic Systems Project Office	Washington, D.C.	SSP-20	
		SSP-24	
		SSP-27	
		SSP-272	
NAVELEXSYSCOM, Navy Space Projects Office	Washington, D.C.	PME 106	
Office of Naval Research	Washington, D.C.	463	
Laboratories			
Naval Surface Weapons Ctr.	White Oak, Md.	Library	
	Dahlgren, Va.	NOL-034	
		Library	
NRL	Washington, D.C.	2027	
		6500 (W. R. Sooy)	
		6506 (H. Gandy)	
Facilities			
NEODF	Indian Head, Md.		
Naval Ordnance Station	Indian Head, Md.	EDL	
NSWSES	Port Hueneme, Cal.	Tech. Library, Code 5100	
		Eng. Directorate, Code 4000	
		Talos Dept., Code 4600	
Schools			
U.S. Naval Academy	Annapolis, Md.	Weapons Dept.	
Naval Postgraduate School	Monterey, Cal.	Library, Tech. Rpts. Sec.	
Naval Guided Missile School	Dam Neck, Va.	Library	
Pac. Flt. Missile Weap. Sys. Trg. Unit	San Diego, Cal.	Library	
Mare Is. Nav. Schools Command	Vallejo, Cal.	Guided Missile School	

*Initial distribution of this document within the Applied Physics Laboratory has been made in accordance with a list on file in the APL Technical Publications Group.

INITIAL DISTRIBUTION EXTERNAL TO THE APPLIED PHYSICS LABORATORY*

TG 1271

ORGANIZATION	LOCATION	ATTENTION	No of Copies
Department of the Navy (cont'd)			
Centers			
NMC	Pt. Mugu, Cal.	Tech. Library 5632.2	
Naval Intelligence Support Ctr.	Washington, D.C.	Aerodyn. Lab. Library	
NWC	China Lake, Cal.	406	
		45	
		Tech. Library, 753	
NELC	San Diego, Cal.	Library	
Naval Ammunition Production Eng'g Ctr.	Crane, Ind.	Naval Ammo. Depot	
Department of the Air Force			
Laboratories			
Aero. Propulsion Lab.	WPAFB, Ohio	F. D. Stull	
Avionics Lab.	WPAFB, Ohio	AVO-2	
Rocket & Propulsion Lab.	Edwards AFB, Cal.	RPMMM	
		MKCO	
Centers			
Arnold Eng'g Devel. Ctr. (AFSC)	Arnold AFS, Tenn.	DSC/Research, AER	
DMA Aerospace Ctr.	St. Louis, Mo.	PRA	
		PDEG	
Hq., AF Special Communications Ctr.	San Antonio, Texas	TDT	
Commands			
Air Force Systems Command	Andrews AFB, Md.	SCTSP	
		Tech. Libr./DPSL	
Air University	Maxwell AFB, Ala.	Tech. Library	
Department of the Army			
Commands			
Missile Command	Redstone Arsenal, Ala.	AMCPM-MDEM	
Centers			
Redstone Scientific Info. Ctr.	Huntsville, Ala.	Chief, Doc. Section	
Laboratories			
Army Ballistic Research Labs.	Aberdeen Proving Ground, Md.	AMXBR-XM-SE	
Arsenals			
Hq., Picatinny Arsenal	Dover, N.J.	STINFO	
U.S. GOVERNMENT AGENCIES			
Security Agencies			
Central Intelligence Agency	Washington, D.C.	CSR/ADD/Std. Dist.	
National Security Agency	Ft. Meade, Md.	C3/TDL	

*Initial distribution of this document within the Applied Physics Laboratory has been made in accordance with a list on file in the APL Technical Publications Group.

INITIAL DISTRIBUTION EXTERNAL TO THE APPLIED PHYSICS LABORATORY*

TG 1271

ORGANIZATION	LOCATION	ATTENTION	No of Copies
U.S. GOVERNMENT AGENCIES (cont'd)			
National Aero. and Space Admin.			
Headquarters	Washington, D.C.	RAP- N. Rekos (Code RLC)	
Hq., Office of Space Sciences	Washington, D.C.	M. J. Aucremanne (Code SG)	
Langley Res. Ctr.	Hampton, Va.	K. F. Rubert J. Henry	
Lewis Res. Ctr.	Cleveland, Ohio	E. Lazberg	
Flight Res. Ctr.	Edwards AFB, Cal.	J. Nugent (Prop.)	
Ames Res. Ctr.	Moffett Field, Cal.	F. Pfyle 228.7	
NASA Scientific and Technical Information Facility	College Park, Md.	J. Waldo	
Goddard Space Flight Ctr.	Greenbelt, Md.	Library - 252	
CONTRACTORS			
Automation Industries/Vitro Labs. Div.	Silver Spring, Md.	Report Acquis. ISA-14	

*Initial distribution of the document within the Applied Physics Laboratory has been made in accordance with a list on file in the APL Technical Publications Group.